

Article

# Horizontal Circulation Patterns in a Large Shallow Lake: Taihu Lake, China

Sien Liu <sup>1,\*</sup>, Qinghua Ye <sup>1,2</sup> , Shiqiang Wu <sup>3</sup> and Marcel J. F. Stive <sup>1</sup>

<sup>1</sup> Department of Hydraulic Engineering, Delft University of Technology, 1, Stevinweg, 2628 CN Delft, The Netherlands; qinghua.ye@deltares.nl (Q.Y.); m.j.f.stive@tudelft.nl (M.J.F.S.)

<sup>2</sup> Deltares, Boussinesqweg 1, 2629 HV Delft, The Netherlands

<sup>3</sup> State Key Laboratory of Hydrology-Water Resources and Hydraulic Engineering, Nanjing Hydraulic Research Institute, Nanjing 210029, China; sqwu@nhri.cn

\* Correspondence: s.liu@tudelft.nl; Tel.: +31-(0)1527-89451

Received: 9 May 2018; Accepted: 13 June 2018; Published: 15 June 2018



**Abstract:** Wind induced hydrodynamic circulations play significant roles in the transport and mixing process of pollutants and nutrients in large shallow lakes, but they have been usually overlooked, while environmental, biological, and ecological aspects of eutrophication problems get the most focus. Herein we use a three-dimensional model, driven by steady/unsteady wind, river discharge, rainfall, evaporation to investigate the spatially heterogeneous, large-scale hydrodynamic circulations and their role in transporting and mixing mechanisms in Taihu Lake. Wind direction and velocity determines the overall hydrodynamic circulation structure, i.e. direction, intensity, and position. A relative stable hydrodynamic circulation pattern has been formed shortly with steady wind (~ 2 days). Vertical profiles of horizontal velocities are linearly correlated to the relative shallowness of water depth. Volume exchange between subbasins, influenced by wind speed and initial water level, differs due to the complex topography and irregular shape. With unsteady wind, these findings are still valid to a high degree. Vertical variations in hydrodynamic circulation are important in explaining the surface accumulation of algae scums in Meiliang Bay in summers. Vorticity of velocity field, a key indicator of hydrodynamic circulation, is determined by wind direction, bathymetry gradient, and water depth. The maximum change of velocity vorticity happens when wind direction is perpendicular to bathymetry gradient. Furthermore, Lagrangian-based tracer transport is used to estimate emergency pollution leakage impacts, and also to evaluate operational management measurements, such as, the large-scale water transfer. The conclusion is that the large-scale water transfer does not affect the hydrodynamic circulation and volume exchanges between subbasins significantly, but succeeds to transport and then mix the fresh, clean Yangtze River water to a majority area of Taihu Lake.

**Keywords:** hydrodynamic circulation; large shallow lakes; vorticity of velocity; wind-induced current; Taihu Lake

## 1. Introduction

Large shallow lakes, especially those located in highly developed areas, provide multifunctional services for industry, agriculture, navigation, and recreation; unfortunately, they have often suffered from severe eutrophication problems [1–3]. In general, population density around these lakes is high [2,4,5], which leads to an additional high waste water and associated nutrients load [6]. These issues have triggered increasing attention for the restoration of the water quality and ecological status of large shallow lakes. The shallowness of lakes is usually emphasized, since the total volume is usually small, and shallow lakes are more sensitive to the effects of wind, evaporation, and human interference, compared to the relatively deep lakes [7–9].

There are two common approaches for shallow lake restoration nowadays. One rather effective approach is to control the source, and thus, to decrease the total nutrient load [10,11], while the other approach is to increase the hydrodynamic circulation [12]. Especially in densely populated areas, source control almost reaches the limit of present technology, whereas enhancing the hydrodynamic circulation might offer an important contribution to improve the water quality of shallow lakes. However, comparing research on hydrodynamics in oceans, coastal zones, rivers, and deep lakes [13], only limited attention has been paid to the hydrodynamics of large shallow lakes. In fact, thorough qualitative studies on horizontal circulation patterns of large shallow lakes are rather scarce, and quantitative studies are even more surprisingly rare. Especially due to their shallowness, the dominant hydrodynamic processes and the corresponding ecosystem in shallow lakes differs very much from that in deeper lakes [14,15]. In deep lakes and reservoirs, due to the large depth, the temperature profile is determined by thermal stratification and mixing that dominates the hydrodynamics, especially the vertical exchange [15], while in large shallow lakes, stratification is seldom observed, which results in substantially different processes.

In large shallow lakes, i.e., with a mean depth <3 m [15], water quality and eutrophication problems are closely related to advection and diffusion processes driven predominantly by wind forcing [16–18]. Momentum transferred by the wind via surface shear stresses generates waves, currents, and associated turbulence [19,20]. While these processes are essentially three-dimensional, the shallowness allows for a depth-averaged, two dimensional representation for some process features [21–24]. Currents induced by wind forcing with velocities at the 10 cm/s scale can lead to lake-wide horizontal circulation patterns with the potential of creating vertical circulations, such as Langmuir circulations [20]. Furthermore, momentum transferred to the bottom will stir up sediment and keep it suspended by turbulence [18,25]. During the suspension and resuspension of sediments, pollutions and nutrients attached to the sediment are released into water column and then transported and mixed by the large-scale circulation [7,26,27]. Thus, the spatial and temporal large-scale, shallow lake horizontal circulation is essential for system understanding before we move to water quality and aquatic ecosystem issues.

In this paper, the focus is therefore on the spatiotemporal wind driven circulations in Taihu Lake, an unusual, extremely shallow and geometrically complex lake including bays and islands (Figure 1). Enhanced anthropogenic emissions in recent years, have had a huge impact on water quality and strongly motivated the eutrophication [28]. Quite some studies have been carried out to seek solutions for the water quality issue of Taihu Lake. One of the most famous engineering interventions is the water transfer project, which diverts water from the Yangtze River of better water quality but more suspended sediment though to the lake, to dilute the excess nutrients and pollutions in the lake water. However, whether the water transfer project has succeeded in improving the general water quality in Taihu Lake remains unclear, since a positive influence could only be observed in some parts of the lake [29,30]. These facts indicate that a better understanding of the hydrodynamics of Taihu Lake is urgently required for future water quality management and restoration of the lake ecosystem. In this paper, numerical models are used to study the hydrodynamics and water quality of Taihu Lake under steady and unsteady wind conditions. Even though, over 20 studies have been carried out using two or three-dimensional numerical models before this study, their focus is either on the resulting water quality index or on the ecological status, and none of them are dedicated to a thorough, quantitative description of (wind induced) large-scale hydrodynamic circulation itself, nor to the implication of hydrodynamic circulation to environment or ecology in this lake [25,31,32].

In this research, hydrodynamic circulation in shallow lakes is defined as the spatially heterogeneous large-scale movement of water. Velocity vectors and particle tracers are used to indicate the hydrodynamic circulation patterns. Timescales are usually from days, weeks, to seasons, and spatial scales can be a few kilometers. Thus, barotropic seiches (~1 day), wind-driven short waves (~seconds), and other processes of smaller timescale are not included in this study.

The overall goal of this study is to gain a better understanding of the wind-induced hydrodynamics, and thereby to provide essential knowledge for the design and implementation of future lake restoration measurements, using state-of-the-art numerical models as a quantitative assessment tool.

Thus, our objectives in this work are: 1. To investigate the rich structure of spatial and temporal varying hydrodynamic circulation (i.e., direction, intensity and position) in a large shallow lake with complex geometry and irregular shape; 2. To quantify wind induced changes in hydrodynamic circulations (volume exchange between subbasins and vertical variations) on spatial scales; 3. To discuss implications of anthropological effects, such as large scale water transfer, on hydrodynamic circulations.

## 2. Study Area Description

### 2.1. Study Area

Taihu Lake is the third largest shallow lake in China with a surface area of 2338 km<sup>2</sup> [32,33]. It is confronted with severe eutrophication problems. Adverse meteorological conditions and increasing waste loads, in combination with the typical geometry of Taihu Lake, with the deepest part no more than 3 m (Figure 1b), cause frequent blooming of algae, with a disastrous impact on the ecosystem. Due to its geographical location in the Yangtze River floodplain, the Taihu Lake Basin belongs to the most populated and economically developed regions in China [25]. The lake provides services such as water supply, flood control, navigation, and recreation etc.

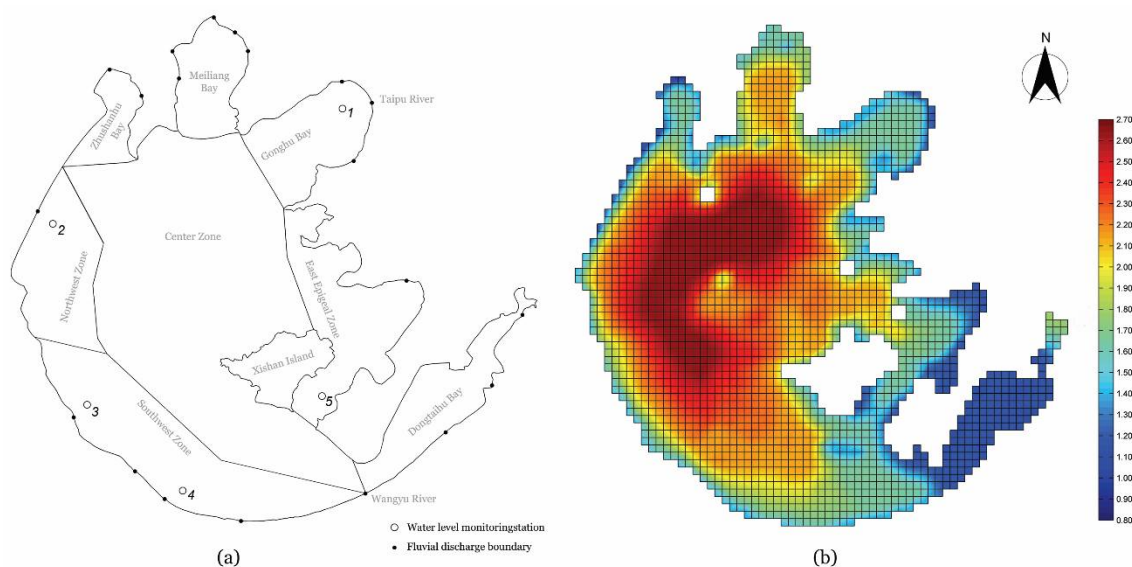


**Figure 1.** (a) Eight subzones, boundary discharge locations, cross-sections and positions of 5 monitoring stations, namely, 1. Wangting Station; 2. Dapukou Station; 3. Jiapu Station; 4. Xiaomeikou Station; 5. Xishan Station. (b) Grid and depth used in numerical model, depth unit: m.

In the area, there are over 150 river tributaries connecting to Taihu Lake. Some of these are very seasonal. Here, we schematized all these branches into 20 discharge boundaries (Figure 1a). Based on the lake's geometrical and hydrological features and ecological functions, Taihu Lake is divided into eight subbasins, namely Gonghu Bay, Meiliang Bay, Zhushan Bay, Northwest Zone, Southwest Zone, Dongtaihu bay, East Epigeal Zone, and Centre Zone [30,33].

Like other large shallow lakes, the hydrodynamics of Taihu Lake are more prone to be altered by wind forcing, evaporation, precipitation, and human interference, etc. The dominant wind direction

over the lake area in summer is southeasterly and reverses in winter, both directions having a large fetch length. Average wind speeds range from 3.5 m/s to 5 m/s [25].

## 2.2. Fluvial Discharge

In situ monthly averaged discharge data of the 20 discharge boundaries schematically representing over 150 river tributaries connected to Taihu Lake are provided by the Taihu Basin Authority. Due to the higher altitude of mountainous area to the west of Taihu Lake, most of the inflow boundaries are located in the northwestern part of the lake. The water transferred from the Yangtze River is injected via Taipu River at northeast of the lake, and further effluent flow goes through the Wangyu River (Figure 1a). Monthly total discharges and corresponding average total water depths in 2008 are shown in Figure 2.

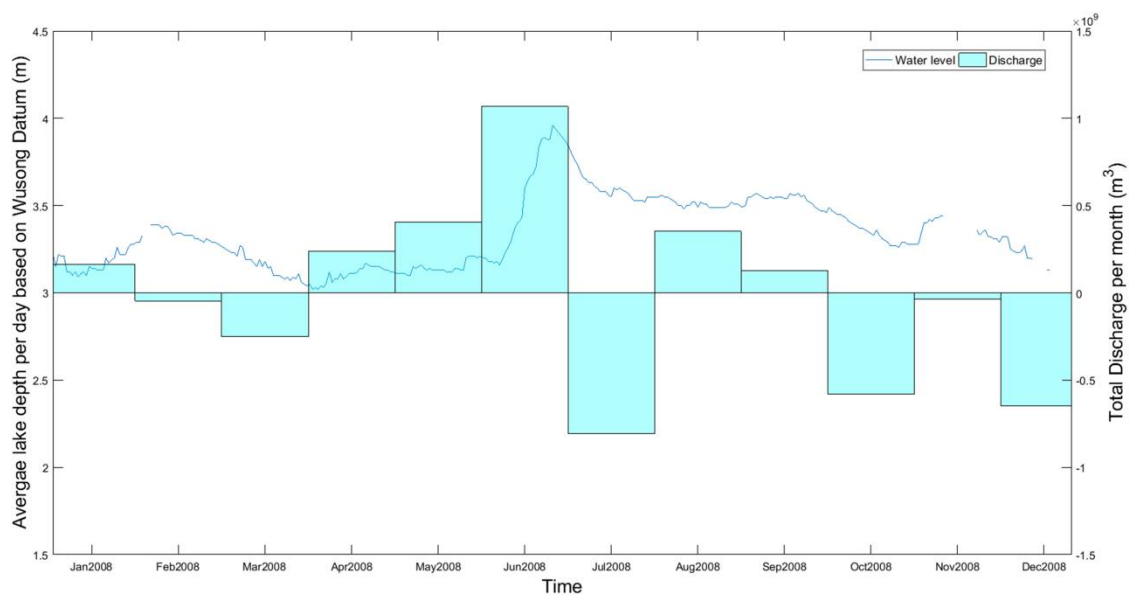


**Figure 2.** Monthly discharge data (bars, positive values represent inflow discharge) and average daily water level (blue line) of Taihu Lake in 2008.

## 2.3. Wind, Precipitation, and Evaporation

The meteorological factors, namely wind, precipitation, and evaporation play significant roles in altering the hydrodynamics and water quality status of the lake. The momentum transferred from wind and water quantity variations due to precipitation and evaporation have a large influence on the consequent hydrodynamic condition. For this model research, timeseries data of 10 m U- and V-wind speed, precipitation, and evaporation is obtained from the website of National Oceanic and Atmospheric Administration of U.S., with frequency of four times a day. Specially for the wind speed, the data are generated onshore, so a correction of 1.2 is applied (cf. Coastal Engineering Manual). The wind shear stress over the lake surface drives the momentum transfer from wind to water. The magnitude of the wind shear stress in this study is approximated by Equation (1):

$$\tau_s = \rho_a C_D |U_w| U_w, \quad (1)$$

where  $\rho_a$  is the air density which is chosen  $1 \text{ kg/m}^3$ ,  $C_D$  is wind drag coefficient, and  $U_w$  is the wind velocity vector, which is measured 10 m above the water surface. The magnitude of the wind drag

coefficient depends on the wind speed [34]. At free surface, the boundary conditions of the numerical model for momentum transfer are

$$\frac{\nu_V}{H} \frac{\partial u}{\partial \sigma} \Big|_{\sigma=0} = \frac{1}{\rho} |\tau_s| \cos(\theta), \quad (2)$$

$$\frac{\nu_V}{H} \frac{\partial v}{\partial \sigma} \Big|_{\sigma=0} = \frac{1}{\rho} |\tau_s| \sin(\theta), \quad (3)$$

where  $\nu_V$  the vertical eddy viscosity,  $u$  and  $v$  are the horizontal velocity components,  $H$  is water depth,  $\theta$  is the angle between the wind stress vector and the local direction of the gridline  $\eta$  s constant.

The yearly total amounts of discharge, precipitation, and evaporation volume of the year 2008 are calculated and used as input for the mass balance check (Table 1). The total volume of Taihu Lake is derived from bathymetry data. Total inflow and outflow discharge is the summation of data of 20 tributaries around Taihu Lake. Rainfall and evaporation volumes are calculated from the daily meteorological data from NOAA.

**Table 1.** Mass balance check using a box model.

Water Mass Balance Check in 2008 of Taihu Lake	Units $10^9 \text{ m}^3$
Total volume of Taihu Lake	4400
Inflow from discharge inlets	11.400
Outflow from discharge inlets	11.416
Rainfall volume	4907
Surface evaporation volume	5186
Error of mass balance	0.294
Relative error *	6.69%

\* The relative error is the ratio of error of mass balance of lake volume and the total volume of the lake.

### 3. Model Description

#### 3.1. Numerical Model Description

The open source three-dimensional shallow water numerical model Delft3D (Delft, The Netherlands), developed by Deltares, is used in this study. Delft3D consists of various modules, covering different physical processes, ranging from flow, sediment transport, morphology to water quality, aquatic ecology, and particle tracking, etc. The model has been extensively applied worldwide in the fields of hydrodynamics, sediment transport, morphology, and water quality in fluvial, lacustrine, estuarine, and coastal environments. In this study, the model is used to simulate the hydrodynamics of the lake for the purpose of illustrating the spatial and temporal large scale hydrodynamic circulation of Taihu Lake induced by the wind shear stress, and the discharge from the tributary rivers given the complex geometry and shallow bathymetry of the lake.

### 3.2. Model Setup

A Cartesian rectangular computational grid is used with grid resolution of 1000 m and total grid number of 9660 (Figure 1). Five vertical sigma layers are defined uniformly for three-dimensional scenarios. For Taihu Lake, the deepest point of the lake appears in the lake center area at 2.66 m, while the shallow points are located close to shorelines, having a typical depth of 0.8 m.

The reference scenario simulates the hydrodynamics of the lake over the entire year of 2008. The simulation time step is based on the Courant–Friedrichs–Lewy (CFL) number and the grid size. To ensure model stability and accuracy, the time step is set to be 5 min. The output time step for observation points is 60 min.

### 3.3. Tracer Redistribution Calculation

Conservative tracers are used in this numerical study to simulate and illustrate the temporal and spatial scale of the hydrodynamic circulation throughout Taihu Lake induced by wind. Conservative tracers do not decay with time and space, and are only passively transported and mixed with hydrodynamics. In this study, when initially released, they are uniformly distributed in the water column. In Delft3D, the principle of simulating the tracer movement is to describe both the advection and the diffusion processes. The lateral term could be realized by giving an additional random movement other than the advective movement in each time step. Size and direction of the movement is proportional to the horizontal and vertical diffusion. Tracers were released in each subbasin in the model area at a constant rate of  $5 \text{ kg/m}^3$  for duration of 3 months. The tracer model results will be further discussed in Section 5.

### 3.4. Model Calibration

The numerical model calibration uses meteorological data and boundary river discharge data for the entire year of 2008. For bottom roughness, we use the Chezy formula, with the roughness coefficient assumed constant at  $65 \text{ m}^{1/2}/\text{s}$  for the entire lake. Horizontal viscosity is set to be  $0.002 \text{ m}^2/\text{s}$  based on literature [35]. For vertical turbulent transport process, a standard  $k-\epsilon$  turbulence model is used.

For model calibration, in situ measurements of water levels from five monitoring stations across the lakes (for locations see Figure 1; data source Taihu Basin Authority) are compared to the simulated results in Figure 3. These five monitoring stations are, namely, Wangting station, Dapukou station, Jiapu station, Xiaomeikou station, and Xishan station. Water levels were observed once a day at each station with occasional interruptions.

Figure 3 show that although the five monitoring stations are located in different parts of the lake, the water levels show very similar trends. Considering the water level difference due to wind setup over the largest fetch length in Taihu Lake with constant  $5 \text{ m/s}$  wind at  $\sim 5 \text{ cm}$  scale, and given the comparison of tributary discharge and average water level trends (Figure 2) with the mass balance check result (Table 1), water levels in Taihu Lake are predominately modulated by tributary discharge, precipitation, and evaporation. The water levels had a slight increase until mid-February, and reached an annual peak value at the beginning of July, then gradually fell to 0 at the end of the year. The highest water level of the whole lake reaches around 1 m, while the lowest water level is around 0 m at the beginning of April. A summary of quantitative model performance indicators are listed in Table 2.

Model performance indicators indicate that the simulation results and in situ measurement for each observation station differ only by a few centimeters, which demonstrates that the model well reflects the water level trend due to the influence of various sources, including tributary discharge, precipitation, and evaporation. The largest variance between modelled and measured water level is in Wangtingtai Station, potentially because of the irregular lake margin near the station. Further sensitivity analysis shows variation of other parameters, like bottoms roughness contributes little to the water level model results.

**Table 2.** Model performance indicators for calibration scenario.

Model Performance Indicator	Dapukou	Jiapu	Xiaomeikou	Xishan	Wangtingtai
RMS error (cm)	11.1	8.6	7.2	5.1	5.4
Error Range (cm)	−16.5~15.8	−18.4~20.9	−31.1~11.6	−29.6~22.8	−41.7~11.6
Mean Absolute Error (cm)	4.3	4.0	5.9	7.5	9.6
Agreement index <sup>1</sup>	0.88	0.89	0.84	0.79	0.75
Model efficiency <sup>2</sup>	0.93	0.94	0.89	0.84	0.77

<sup>1</sup> The Nash–Sutcliffe index of efficiency from [36]; <sup>2</sup> The index of agreement from [37].

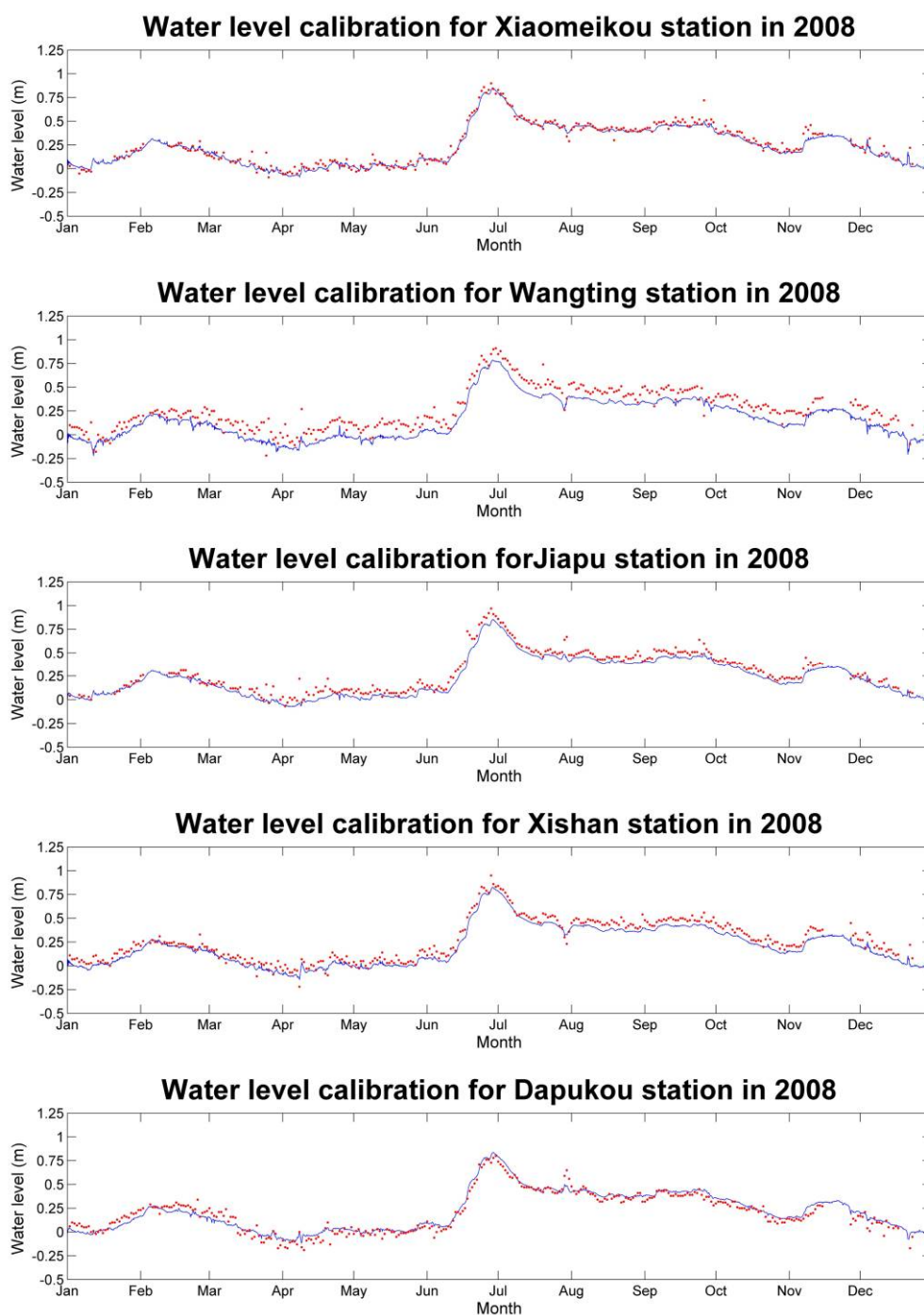


**Figure 3.** In situ measured and modeled water level for five monitoring stations in 2008, water levels are based on Wusong Datum. Measured levels are shown with points, and model results are shown with solid lines.

## 4. Results

### 4.1. Steady Wind

#### 4.1.1. Effects of Wind

Besides the fluvial discharge for the tributaries into the lake, wind forcing is an important momentum source driving hydrodynamic circulations. Wind data analysis and literature show that the prevailing wind is from southeast in summer and from northwest in winter. Since Taihu Lake is located in a typical monsoon climate zone characterized by prevailing southeast wind in summer and northwest wind in winter, the wind direction is relatively consistent at a timescale of days [28,33]. The average wind speed is ~5 m/s. To see the wind influence on the hydrodynamic circulation, we used steady wind of 5 m/s and 10 m/s wind speed from summer and winter prevailing wind directions. Depth-averaged circulation gyre pattern, volume exchange rates between subbasins, and the big lake and vertical variations are examined.

With constant wind, the depth-averaged hydrodynamic circulation gyres and surface water level slope in the lake takes around 2 days to reach a rough steady state. Thus, a relatively stable hydrodynamic circulation gyres pattern can be achieved (Figure 4).

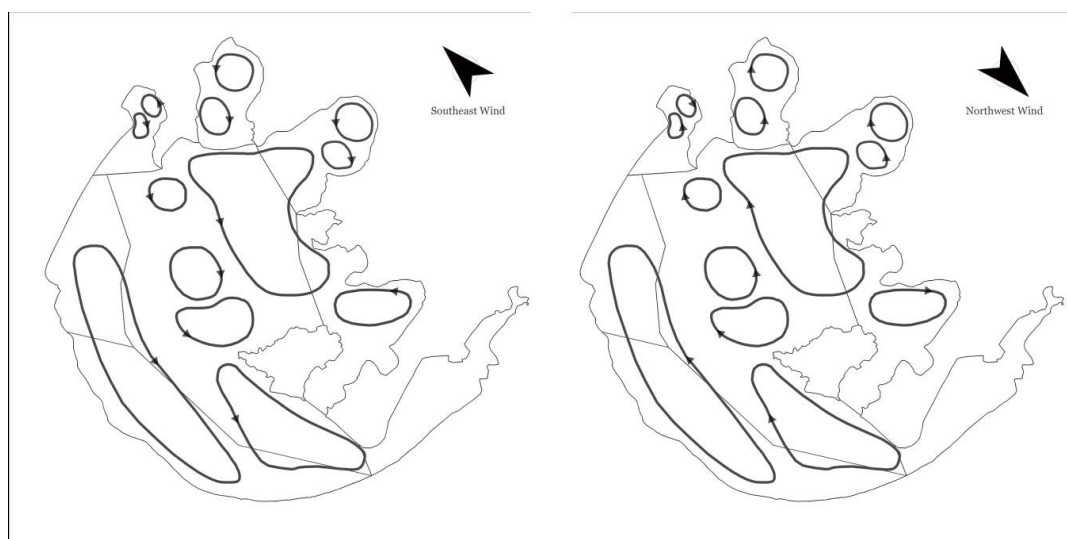


**Figure 4.** Depth-averaged circulation gyres for northwest and southeast wind.

In the three northern subbasins, the structures of hydrodynamic circulation are similar where two half-subbasin-sized scale circulation gyres with opposite directions are formed. The directions of the inner circulation gyres are clockwise for northwest wind, and counterclockwise for southeast wind. Along the entrance line of all three subbasins, current velocity is relatively large with either eastwards or westwards direction. With constant northwest wind, the flow goes eastwards, while with the southeast wind, the flow reverses. In the East Epigeal Zone, except for the eastern corner, a near-shore current with high velocity flows near the eastern margin of Taihu Lake, in the same direction as the wind. In the eastern corner, a circulation gyre appears. For the northwest wind, the gyre is clockwise, while for the southeast wind it is counterclockwise. In the Centre Zone of the lake, 5 smaller scale circulations occur due to the combination effects of a strong current in the southwest and the topographic limitation of Xishan Island. Near the entrance of Dongtaihu Bay, at the southern margin of the lake, the current direction is opposite to the east–west component of the wind direction. An elongated-shape circulation crossing the Northwest Zone, the Southwest Zone with high current velocity is observed. Direction of this circulation gyre is clockwise with southeast wind and counterclockwise with northwest wind.

The rich structure of the steady hydrodynamic circulations is caused by the combined effects of the irregularly shaped subbasins and the overall complex geometry. In the shallower margin of the lake parallel to the wind direction, the flow direction is the same as the wind. In the deeper central zone of the lake, there are currents with smaller velocity flowing opposite to the wind direction. Two main circulation gyres are stable and consistent throughout the lake, one is in the southwestern part of the lake near the western margin, the other one is around the Center Zone and Xishan Island. The latter one is the largest hydrodynamic circulation at the scale of lake size, and is connected with all the other subbasins around the Taihu Lake. Sediments, nutrients and other suspended matters in the water could be transported from one subbasin to another with this hydrodynamic circulation, hence, it is very crucial for the transport and mixing in the lake.

Volume exchange between subbasins is the accumulated discharge through cross-sections which defined the borders between subbasins. To quantitatively study the initial water level influence on volume exchange between the subbasins in Taihu Lake, the nine cross-sections can be categorized into two types: one type connects a semi-closed subbasin, for example, the entrance cross-section of Meiliang Bay; the other type links two subbasins with an entrance cross-section and a linking cross-section, for example, the cross-sections between Eastepigeal Zone and the Center Zone. Note that the small total volume exchange rate at the first type of cross-section is due to the combined but usually reversed effect of surface and bottom flux, which is the result of the topographic limitation and semi-closed subbasin shape. For the second type, the total volume exchange is much larger. Directions of volume exchange are directly related with wind direction (Figure 5).

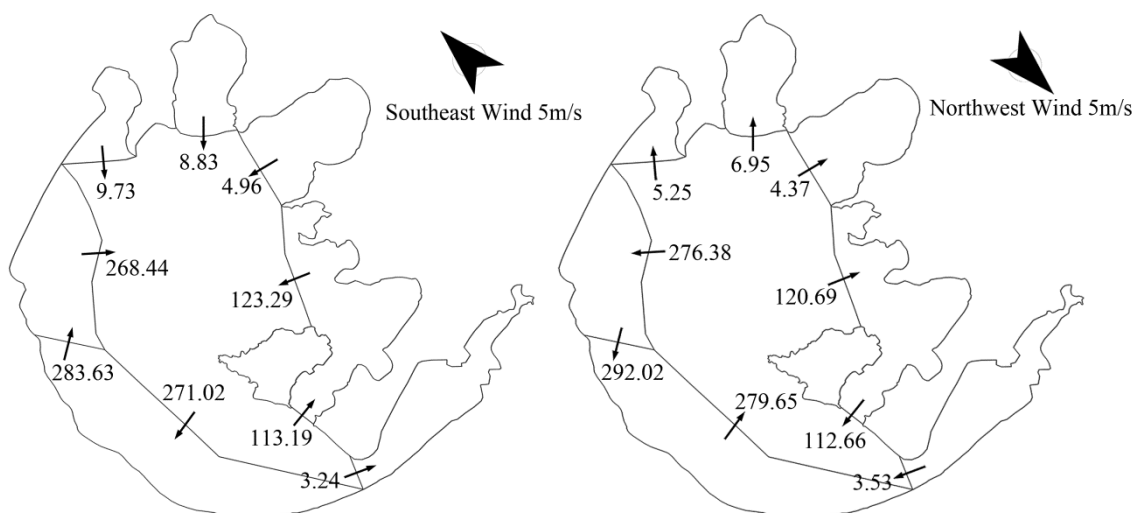


**Figure 5.** Volume exchange between subbasins, with constant wind unit of numbers shown in the figure in  $m^3/s$ .

#### 4.1.2. Effects of History Wet/Dry Season

To study the effects of history wet/dry season impact on the hydrodynamic circulation, different initial water levels are used. The observed water levels of five monitoring stations show a maximum water level difference of around 1 m, with the peak value in summer (Figure 2). Accordingly, the initial water level of 1 m and 0 m are included in numerical simulations.

Model results show that with constant wind, difference in initial water level contributes little to the depth-averaged hydrodynamic circulation patterns. Current velocity varies with initial water depth, but the direction and shape of the hydrodynamic circulation patterns remain unchanged. However, the effect of initial water level with constant wind is more significant in the volume exchange between subbasins. (Figure 6). Volume exchange rates calculation is further explained in Appendix A.

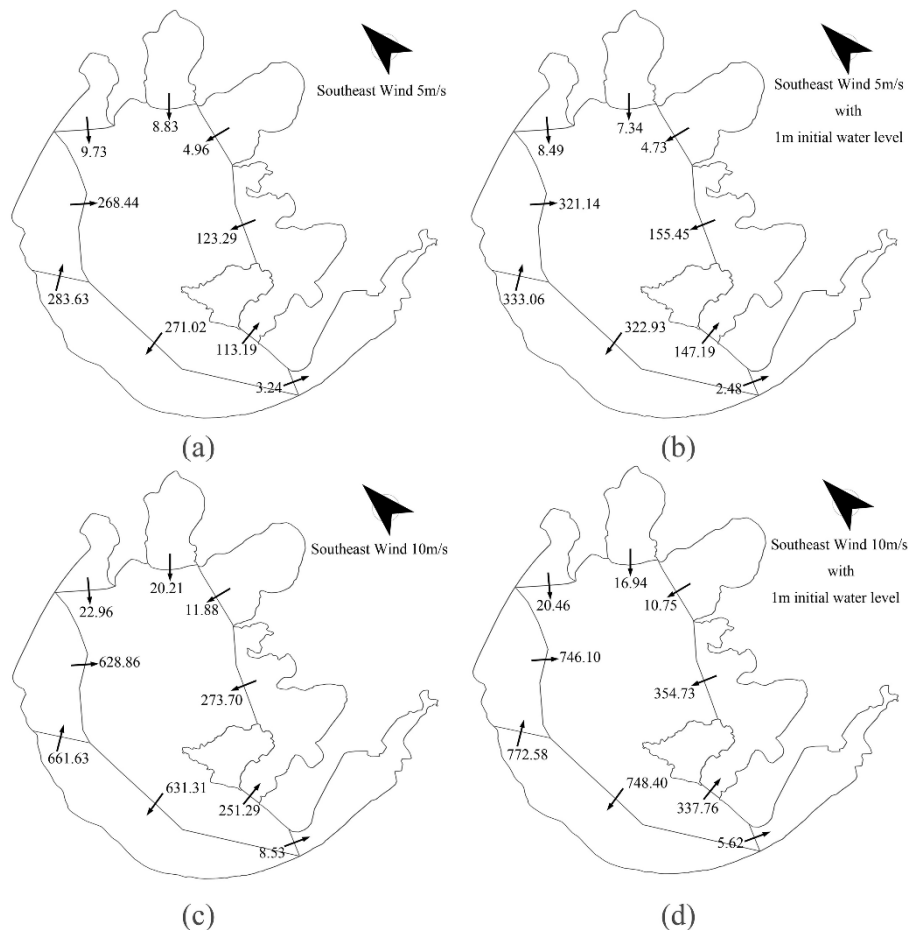


**Figure 6.** Volume exchange rates between each subbasin with southeast wind. Unit of numbers shown in the figure is  $m^3/s$ ; (a) 5 m/s southeast wind scenario; (b) 5 m/s southeast wind and 1 m initial water level scenario; (c) 10 m/s southeast wind scenario; (d) 10 m/s southeast wind and 1 m initial water level scenario.

Effects of the initial water level on total volume exchange at the two types of cross-sections are different. For the first type of cross-section, volume exchange rates decrease with higher initial water level, while for the second type of cross-section, the trend is opposite. These phenomena can be explained by the boundary and bottom limitations. For the first type of cross-section, the semi-closed subbasin behind is restricted by the closed boundaries around it, as well as the narrower entrance. Consequently, the circulation flux is trapped, and higher initial water level increase the difficulty of volume exchange. Meanwhile, for the second type of cross-section, the boundary influence for subbasins that are behind it is relatively smaller, and the bottom influence is less, due to larger water depth than for the first type. A higher initial water depth can weaken the bottom restrictions even more, and thus, induce higher volume exchange rates.

Studying the volume exchange rate at cross-sections indicates the difference between water exchange efficiency during summer and winter time, which is of significant importance for water quality issues. In summer, the water level of the whole lake is roughly 1 m higher than that in winter. For the same wind speed, water in semi-closed subbasins is harder to exchange than in the winter, while for relatively open subbasins, water exchange is enhanced.

#### 4.1.3. Effects of Wind Speed

Similar to initial water level, changing of wind speed does not significantly change the shape of the hydrodynamic circulation. However, the effect of wind speed on the net volume exchange between subbasins is significant. (Figure 6).

Unlike the effect of initial water level, increase of wind speed will consequently induce the increase of net volume exchange between subbasins. With same initial water level and wind direction, increase of the wind speed stimulates the current due to the increase of momentum transferred from wind to water, which in turn, increase the net volume exchange.

#### 4.1.4. Vertical Variation in the Flow Field

In literature, vertical variation of hydrodynamic circulation is usually described as a surface flow following the wind direction, and a compensation flow along the bottom. Due to the complex topography of Taihu Lake and its irregular shape, this simple conclusion is not universally valid for every subbasin within the lake. The details of vertical flow structure will be discussed in this section.

The existence of complex geometry and irregular boundary shape yield a rich three-dimensional flow structure in Taihu Lake. Figure 7 shows the simulated surface and bottom layer horizontal circulation field with constant 5 m/s southeast wind.

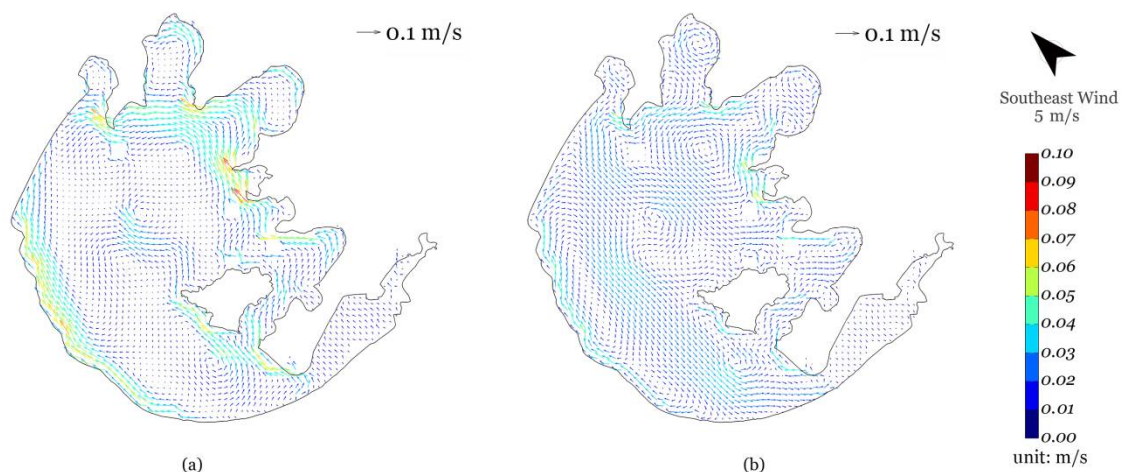


**Figure 7.** Surface and bottom horizontal hydrodynamic circulation pattern with southeast wind, with (a) the surface layer velocity field, (b) the bottom layer velocity field.

The hydrodynamic circulation patterns of surface layer and the bottom layer differ with location. The major flow direction difference occurs in the center zone of the lake, where water depth is relatively larger. Surface layer currents follow the wind direction, while at the bottom, the direction is reversed. Also, at some locations in the deepest area, for example, near the borderline of the southwest zone and the center zone, there are entire water columns from surface to bottom flowing against the wind direction, with the largest flow velocities in the bottom layer.

For the shallower part, like along the western margin of the lake, borders of the three subbasins in the north, as well as the entire Epigeal Zone and Dongtaihu Bay, unlike the conclusions from previous studies, the current in the entire water column follows the same direction, but the surface flow has a larger velocity.

For the three northern subbasins where the algal bloom problem is most severe, the three-dimensional hydrodynamic circulation is more complex, due to the narrow constrictions at the entrance. Figure 8 shows, as an example, the zoomed-in surface and bottom horizontal circulation pattern in Meiliang Bay, where most of the surface flow vectors follow the wind direction, while the bottom current direction is opposite to the wind direction.

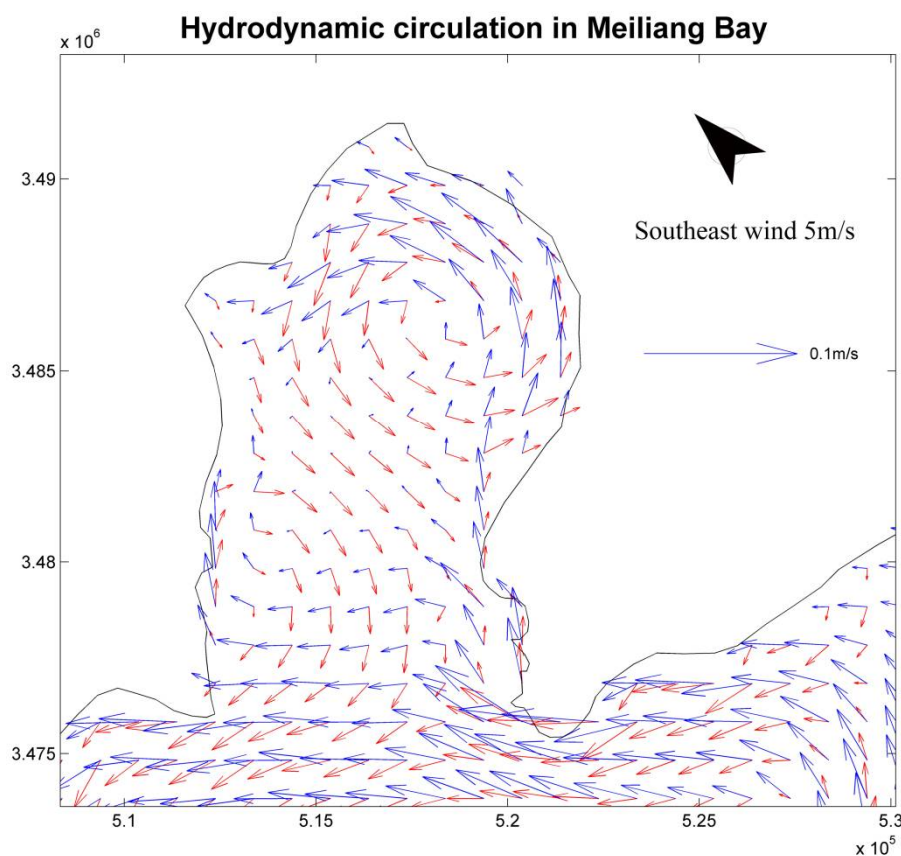


**Figure 8.** Comparison of surface and bottom hydrodynamic circulation pattern of Meiliang Bay of model result of case 2 with 5 m/s constant southeast wind. The blue vector indicate flow pattern on the surface layer and the red vector indicate the bottom layer. The x, y coordinates (m) are based on Beijing 1954 coordinate system.

The hydrodynamic circulation of Meiliang Bay could be interpreted as a scaled-down version of the whole Taihu Lake. The deepest part of Meiliang Bay is in the center, while for the area near the margin, it is shallower. Especially, the western part of the entrance is shallower than the eastern part. Along the shallower northeastern and southwestern margin of the basin, current directions are similar to wind direction, with the surface velocity larger than the bottom velocity. While in the deeper part in the central zone, the flow direction at the bottom reverses. A difference of flow direction at the surface and bottom indicates the presence of a return flow, and thus, a vertical circulation. The return flow structure is observed after two days with wind, holding the same direction.

Variations in the horizontal current velocity have a direct impact on the surface and bottom volume exchange rates through the cross-sections. Except for very narrow and very shallow cross-sections, surface and bottom flux directions are reversed. Directions of surface or bottom volume exchange correlate with the wind direction. For most cross-sections, surface and bottom volume exchange rates increase with wind speed (Figure 9).

The hydrodynamic character of the lake is very similar to the channel shoal system in a fluvial estuary, where the surface water moves in the direction of the driven force, and the reverse flow appears in the deeper channel. This phenomenon can also explain the reason why algae consistently accumulate in the subbasins. In the daytime of spring summer time, toxic algae, such as Chlorophyta, float upward from the bottom for photosynthesis, and stay at the surface layer in the daytime. During the day, the algae are consistently transported by the surface layer current in the prevailing wind directions to the northern subbasins. Since only water in the deeper part has a southern outwards current direction,

the algae keep accumulating with the surface water, and are captured inside Meiliang Bay, which eventually causes the algae bloom.

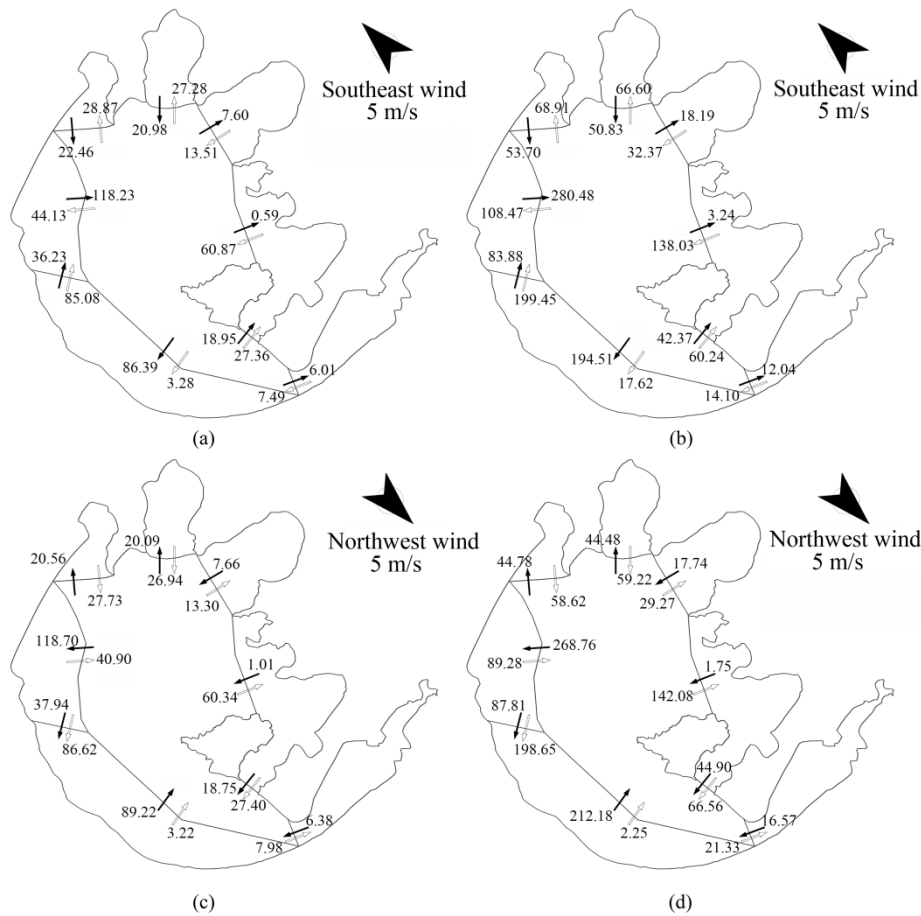


**Figure 9.** Surface and bottom layer flux with constant wind. The hollow arrows represent surface flux, while solid arrows are the bottom flux. (a) Model result with constant 5 m/s southeast wind, (b) model result with constant 10 m/s southeast wind, (c) model result with constant 5 m/s northwest wind, (d) model result with constant 10 m/s northwest wind. Unit of numbers in the figure is  $m^3/s$ .

#### 4.2. Unsteady Wind

Hydrodynamic circulation varies with wind scenarios as indicated by model results shown in Section 4.1. In nature, both wind speed and directions are unsteady. However, the prevailing wind directions around Taihu Lake in summer and winter are relatively fixed, as shown in Figure 10. Observed wind show it could blow persistently at one prevailing direction for a couple of days until it changes direction, while the wind speed changes daily.

The shift from a steady hydrodynamic circulation situation to another due to changing wind takes around 2 days. This process usually coincides with complex and rapid shifting in horizontal hydrodynamic circulation. Major circulation gyres change shape and direction, and so does the water jet along the shallow margin. As discussed in the last section, with the same wind direction, the horizontal circulation pattern is fixed regardless of the wind speed, while wind speed is responsible for the varying volume exchange between each subbasin. Using the reference scenario as an example, bottom and surface layer flux through the nine cross-sections between subzones are shown in Figure 11. Both the directions and the flux value change with wind directions. For most cross-sections, bottom flux and surface flux have the same direction, such as cross-section Eastepigeal 1. However, for cross-sections like entrance of Meiliang Bay, surface and bottom flux are reversed.

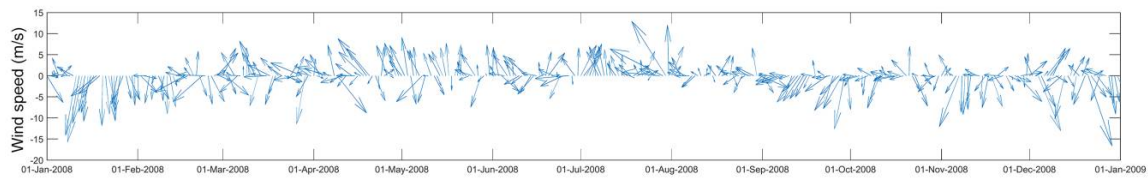


**Figure 10.** Time series of wind vectors of year 2008, with north wind pointing to the top, length of each arrow refers to the wind speed.

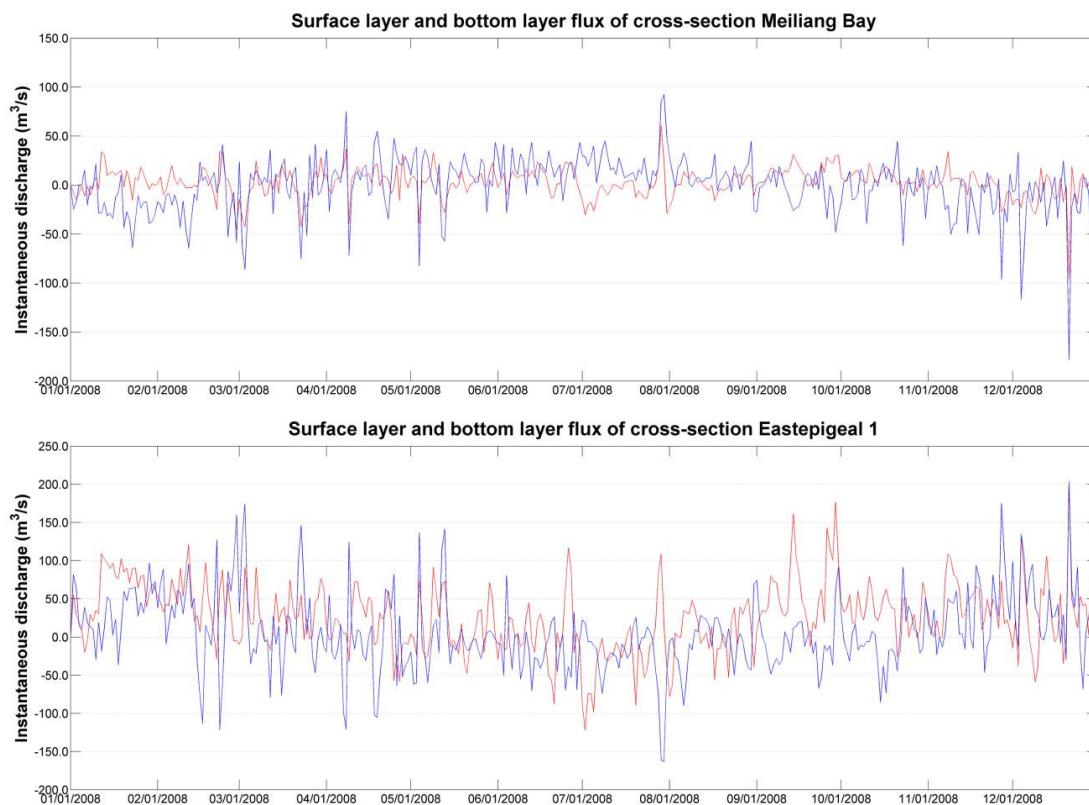


**Figure 11.** Time series of surface and bottom flux of reference scenario (case 1), the red line refers to bottom flux, and the blue line refers to the surface flux, and the unit in the figure is  $\text{m}^3/\text{s}$ .

The flux due to unsteady wind can be further understood from the conclusion of steady wind situation. To illustrate this, the zoomed in total flux and wind records of southwest1 cross-section in April 2008 is shown in Figure 12 as an example.

In the steady wind situation, the stable hydrodynamic circulation occurs after two days of simulation, while in reality, the direction and magnitude of wind changes with time, and so does the total flux through cross-sections. Magnitude of the total flux increases with continuous wind blowing from same direction (17 April to 19 April in Figure 11), while the change of direction of the total flux occurs with wind direction changes (7 April to 8 April). For unsteady wind, the response of the total flux to wind is relatively fast, due to sharp wind changes, and it reaches a similar equilibrium as the steady wind.

To conclude, with unsteady wind condition, although the stable hydrodynamic circulation may not occur due to fast varying wind, the volume exchange patterns and cross-section flux changes with steady wind condition are still, to a high degree, valid.

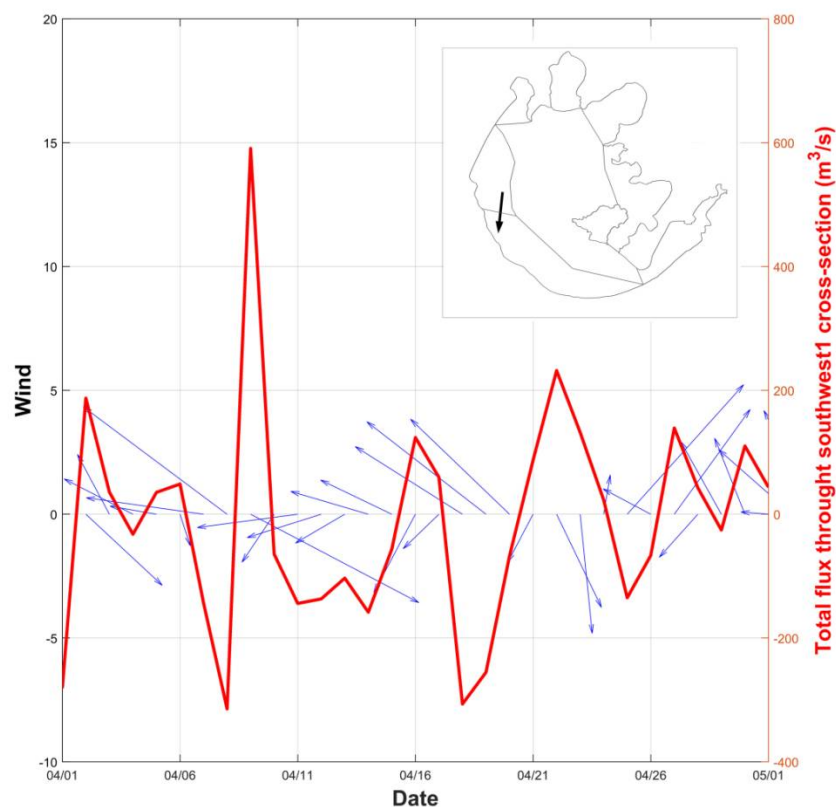


**Figure 12.** Total discharges and corresponding wind vector of southwest1 cross-section in April 2008. The blue vector represents the wind record and the red line represents the total flux through southwest1 cross-section. The length of the blue wind vector is the magnitude of wind speed. The position and the arrow representing the positive flux are illustrated in the upper right subplot.

## 5. Discussion

Wind influence on the hydrodynamic circulations has been discussed above. The Delft3D simulation model is shown to be able to reproduce the spatial and temporal hydrodynamic circulation patterns in Taihu Lake. However, given the uncertainty in numerical and process input parameters and the unique geomorphology of Taihu Lake, these model results should be carefully scrutinized. To evaluate input errors, model sensitivity analyses is provided in Sections 5.1 and 5.2, concerning grid size and bed roughness, respectively. Velocity vorticity, as the key indicator of hydrodynamic circulation, predominantly modulated by wind, depth, bathymetry gradient etc., is discussed through both a theoretical analysis and flat bottom model tests in Section 5.3. Furthermore, Lagrangian-based tracer tests are used to evaluate emergency pollution/leakage effects in Section 5.4, and water transfer effects in Section 5.5.

### 5.1. Grid Size Effects

Before model calibration, sensitivity tests have been carried out to test the influence of numerical parameters. One of the major issues is grid size. In this study, the grid size is chosen to be 1000 m. A grid size of 500 m is utilized in most earlier numerical studies of Taihu Lake. To test the influence of grid size on the model accuracy and efficiency, a 500 m grid size model was set up and model behavior was analyzed (Table 3). In both cases, the chosen time step of 10 min fulfils the courant number requirement.

**Table 3.** Model behavior with 500 m grid size.

Model Performance Indicator	Dapukou	Jiapu	Xiaomeikou	Xishan	Wangtingtai
RMS error (cm)	7.8	8.6	8.8	8.5	8.3
Error Range (cm)	−30.4~13.2	−31.9~27.3	−33.8~10.8	−21.3~7.8	−33.2~11.1
Mean Absolute Error (cm)	6.4	7.2	7.7	7.7	6.7
Agreement index <sup>1</sup>	0.83	0.79	0.80	0.79	0.81
Model efficiency <sup>2</sup>	0.86	0.82	0.83	0.84	0.84

<sup>1</sup> The Nash–Sutcliffe index of efficiency from [36]; <sup>2</sup> The index of agreement from [37].

Model performance for the water level of five monitoring stations with the finer grid of 500 m is listed in Table 3. Results of the sensitivity analysis show the water level variations and hydrodynamic circulation patterns hardly change with grid sizes. Model performances of both models are equally good, while the coarse grid has an advantage in model efficiency. Thus, the 1000 m grid size was chosen.

### 5.2. Bed Roughness

The bottom roughness coefficient is another common tuning parameter in hydrodynamic models. To be noticed, in Delft3D-FLOW, bottom roughness coefficient with other formulas is converted to Chezy coefficient before simulation. Sensitivity analysis on Chezy coefficient ranging from 40 to 80 has been carried out. Results show little change on the hydrodynamic circulation patterns, water level variations, and velocity profiles. Thus, we conclude sensitivity of bottom roughness coefficient is not significant in this case. A default value of Chezy coefficient  $65 \text{ m}^{1/2}/\text{s}$  is chosen. However, if the model is further applied to ecology or sediment dynamics studies, attention should be paid on the bottom roughness since the correlated bed shear stress have a critical impact on the sediment resuspension process.

### 5.3. Velocity Vorticity: Key Indicator of Hydrodynamic Circulation

Vorticity can be used to describe the spatially varying rotational character of a flow field [38]. In this section, we focus on the vorticity of the horizontal velocity field in shallow water as the indicator of hydrodynamic circulation. The appearance of hydrodynamic circulation in the form of vorticity in the Lagrangian horizontal velocity field requires driving forces, which can be the wind shear stress gradients due to inhomogeneity of the wind velocity field, existence of submerged and emergent plants, the Coriolis effects, and the bathymetry variations. The influence of bathymetry variations is noteworthy compared to the other factors mentioned above [39]. In Lake Ontario, Csandy (1973) schematized the study area into a long and narrow lake with parallel depth contours, and proposed the idea of “topographical gyres”, where the depth-averaged current direction is identical to wind direction in the shallow area, and opposite in the deeper area. This phenomenon was also observed in other shallow lakes around the world [19,40,41]. However, these studies mainly focus on long and narrow lakes. For shallow lakes with other shapes and more rugged topography, where lateral differences are more significant, studies are lacking. With different bathymetry and bathymetry gradient, behavior of hydrodynamic circulation in the lake center area and the littoral zone varies (Figure 4).

In previous studies, an analytical solution for the influence of bathymetry on the vorticity has been derived [19,42]. Hereby we present a brief review. Assuming a steady state with constant wind, i.e., the time derivative of horizontal velocity is 0, and the depth-averaged shallow water equations are

$$\nabla \cdot V = 0, \quad (4)$$

$$\nabla U - fV = -g \frac{\partial \eta}{\partial x} + \frac{\tau_{s,x} - \tau_{b,x}}{\rho h} + \nu \cdot \Delta U, \quad (5)$$

$$\nabla V + fU = -g \frac{\partial \eta}{\partial y} + \frac{\tau_{s,y} - \tau_{b,y}}{\rho h} + \nu \cdot \Delta V, \quad (6)$$

where  $V$  is the horizontal velocity vector with  $x$  component  $U$  and  $y$  component  $V$ ,  $f$  is the Coriolis factor,  $g$  is the gravitational acceleration,  $\eta$  is the surface elevation,  $h$  is the total depth,  $\tau_s$  is the surface wind shear stress,  $\tau_b$  is the bottom shear stress,  $\rho$  is the density of water, and  $\nu$  is the horizontal eddy viscosity.  $\nabla$  is the Del operator and  $\Delta$  is the Laplace operator.

Introducing the vorticity of the horizontal velocity,  $\sigma = \nabla \times V = \frac{\partial V}{\partial x} - \frac{\partial U}{\partial y}$ , and taking the  $y$ -derivative of Equation (5) and  $x$ -derivative of Equation (6), together with Equation (4), the governing equation for the vorticity becomes

$$V \cdot \nabla \zeta = -(\zeta + f) \nabla \cdot V + \nabla \times \left( \frac{\tau_s}{\rho h} \right) - \nabla \times \left( \frac{\tau_b}{\rho h} \right) + \nu \Delta \zeta. \tag{7}$$

The first term on the right-hand side represents the vortex stretching, the second term represents the vorticity input from wind, the third term is the vorticity sink due to bottom shear stress, and the last term is eddy-viscosity related. Compared to wind shear stress term, the latter two terms are one or more magnitudes smaller, thus, they are negligible.

With constant water density, the wind vorticity input term becomes

$$\nabla \times \left( \frac{\tau_s}{\rho h} \right) = \frac{1}{\rho} \left( \frac{1}{h} \nabla \times \tau_s - \frac{\tau_s}{h^2} \times \nabla h \right). \tag{8}$$

The first term in the bracket is related to wind stress curl, with constant wind, this term is 0, and a so-called barotropic topographic gyre is generated; the second term represents the velocity gradient influence on the vorticity.

Results from the numerical model also confirm the analysis above. With constant wind from northwest, the depth-averaged vorticity is shown in Figure 13. In the littoral area, where the total water depth gradient is perpendicular to the wind speed, wind generates a large vorticity value. Along the southwest shore in the Taihu Lake, the current direction is the same as the wind, thus, it will produce a counter clockwise horizontal circulation. Even in the same gyre, the vorticity is larger, with the depth becoming smaller. Similar phenomena could be observed in the northeast boundaries of the Lake, the vorticity is negative, which means a clockwise gyre and the shallower part has the larger absolute value of vorticity. For locations where the depth gradient is small, for example, Dongtaihu Bay at the southeast part of Taihu Lake, the vorticity is almost zero.

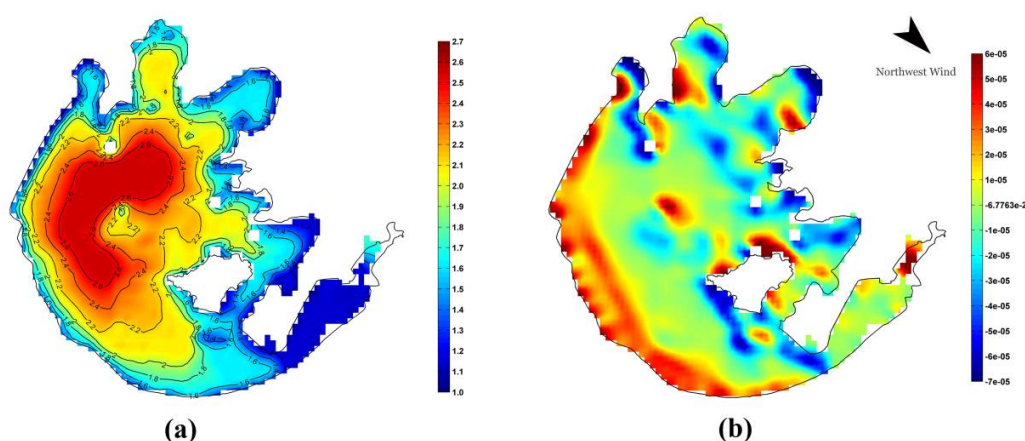


**Figure 13.** (a) Depth contours of Taihu Lake, unit: m; (b) Depth-averaged vorticity with constant northwest wind.

These conclusions can be further illustrated by a numerical test with a flat bottom. Changing the bottom depth to a uniform value of 2 m and maintaining all other parameters yields model results, as shown in Figure 14.

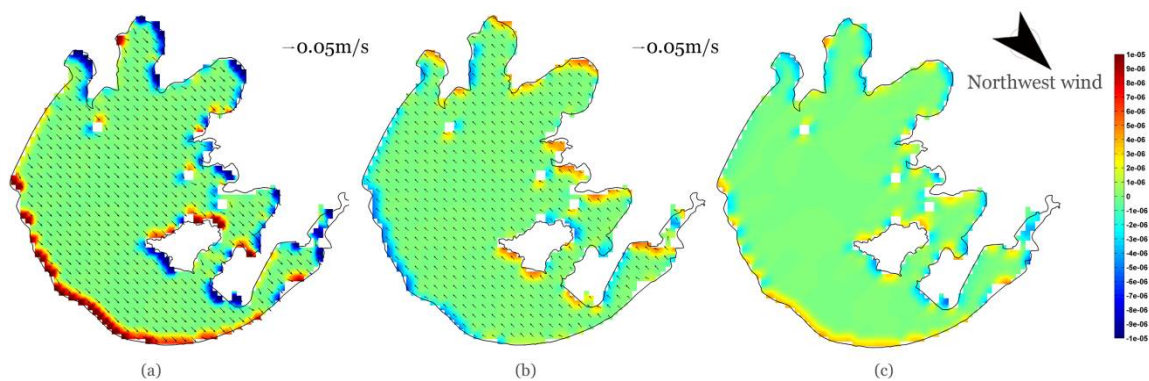


**Figure 14.** Numerical model results of velocity and vorticity with 2 m constant depth and constant northwest wind. The vectors represent velocity and colored patches represent vorticity. (a) Surface layer; (b) Bottom layer; (c) Vorticity of depth-averaged velocity.

With constant depth, except for the grids near the boundary, depth gradients at all locations are zero. Thus, according to Equation (5), the velocity vorticity at each layer should be 0 as well, as illustrated in Figure 14. Along most of the boundaries, for example, the southwest shoreline, the velocities of surface layer and bottom have the same magnitude but opposite directions; thus, the vorticity is positive and negative, respectively. Since the depth-averaged vorticity is the superposition of each layer's vorticity, the values near the boundaries are approaching 0 (see Figure 14c).

It may be concluded, both from the theoretical analysis and numerical tests results above, that the vorticity in the velocity field is related to directions of wind, current, and bathymetry gradient, as well as the value of water depth and wind shear stress. When the current velocity is in the same direction as wind, the major bathymetry influence is the depth gradient and depth itself. Wind has the largest influence on the vorticity when its direction is perpendicular to that of the bathymetry gradient. Wind related vorticity change is larger with larger wind speed and smaller water depth.

#### 5.4. Transport Due to the Horizontal Circulation

Circulation and redistribution of lake water throughout the lake is further illustrated by the model results of the tracer experiment for the first half-year of 2008, with steady wind scenarios. At the beginning of the simulation, the tracer concentration all over the lake is 0. After that, tracers are released persistently in the first three months of the simulation, at a rate of 5 kg/s. Tracers are released at a chosen subbasin for each scenario. Here in this study, depth-averaged tracer concentration is presented.

Tracer movements reflect well the characteristics of the hydrodynamic circulation under steady wind conditions, discussed in Section 4.1, e.g., when taking the tracer releasing experiment in Eastepigeal as a representative example (Figures 15 and 16).

With constant southeast wind, initially, tracers move northwards via the shallow east margin of Epigeal Zone, where the depth-averaged flow velocity in the wind direction is the largest. Subsequently, the tracers penetrate into Gonghu Bay, with the counterclockwise circulation near the entrance of Gonghu Bay (Figure 4). After that, tracers move westerly with the same circulation pattern, and enter the semi-closed subbasins of Meiliang Bay and Zhushan Bay, with smaller subbasin scale circulations. Finally, the tracers move southwards along the deeper center, and spread all over the lake. The entire time for the advection and diffusion process to fully mix the tracers in the entire lake is around 2 months' time. Similarly, with constant northwest wind, tracers' movements follow the hydrodynamic circulation pattern.

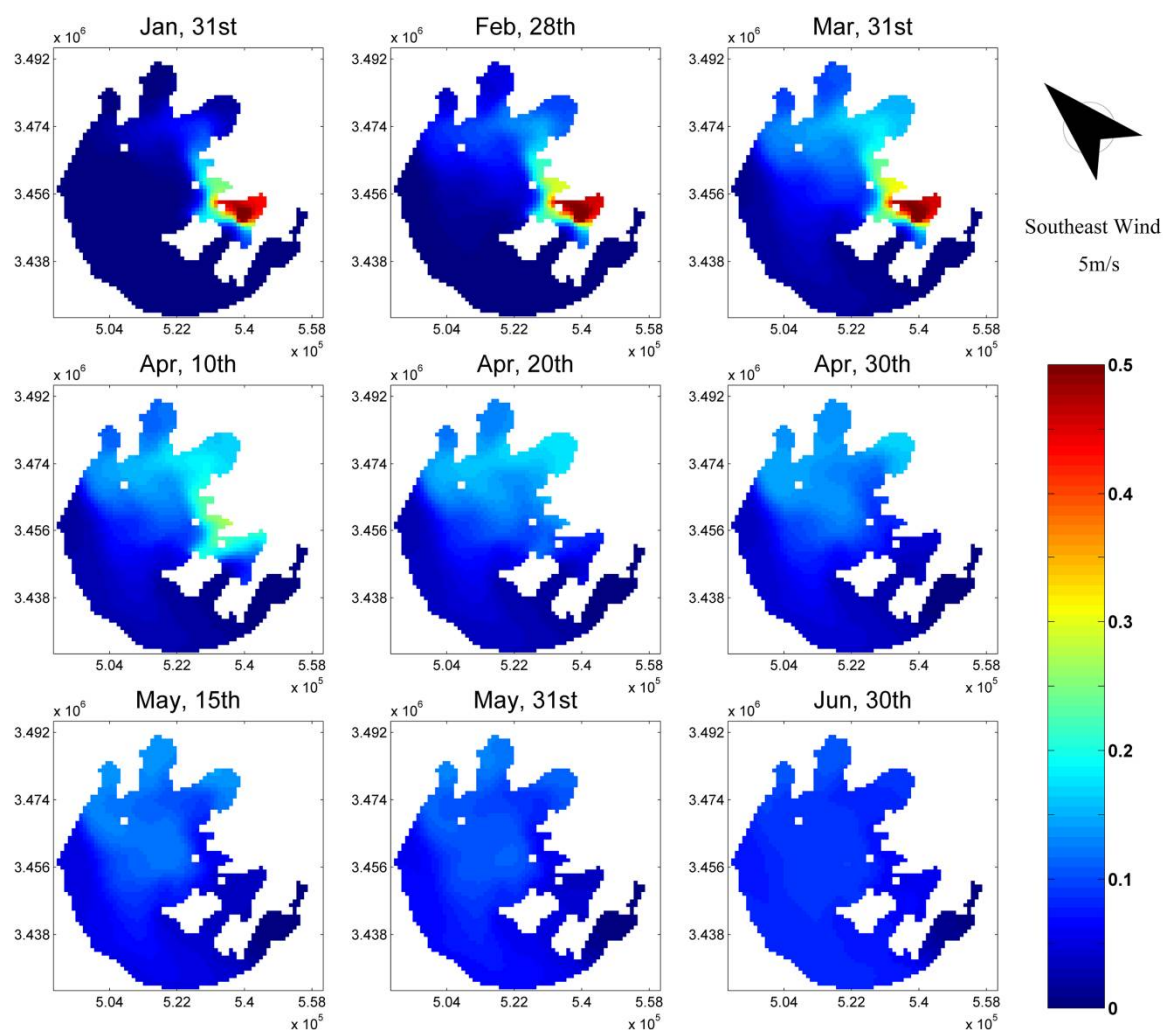


**Figure 15.** Time series of tracer concentration images, with the model driven by constant 5 m/s southeast wind. Unit in the figure is  $\text{kg}/\text{m}^3$ .

However, as shown in Figure 16 on 30 April, tracer concentration is still high at the southern boundary of the lake, which means that for different locations in the lake, the duration of high tracer concentration due to redistribution of lake water by wind effects is different. For lake water quality management, it is crucial to assess the temporal influence at a critical spot of a random pollution emission. Thus, altogether, six important spots are chosen around the lake, including one drinking water intake point [28] and five tourist places, as shown in Figure 17, to analyze the influence of pollution release in the numerical experiment.

Taking spot A as an example, time series of tracer concentration with different release spots are shown in Figure 18. Significant variance in the tracer concentration trend is also the direct result of hydrodynamic circulation, which determines moving trajectory of tracers between the interested location and the releasing spots. Under the constant southeast wind condition, water from Gonghu Bay, Eastepigeal Zone, and Center Zone has the largest influence. Location A lays near the joint point of Meiliang Bay and Gonghu Bay, where a subbasin scale circulation occurs (Figure 4). With southeast wind, this circulation gyre will first drive water from inside the Gonghu Bay to point A. Then, several days later, water from Eastepigeal Zone and Center Zone will join this circulation gyre, and move towards location A, which could also explain why the peak of concentration curve of the latter two releasing is several days after the release stop time on 31st of March.

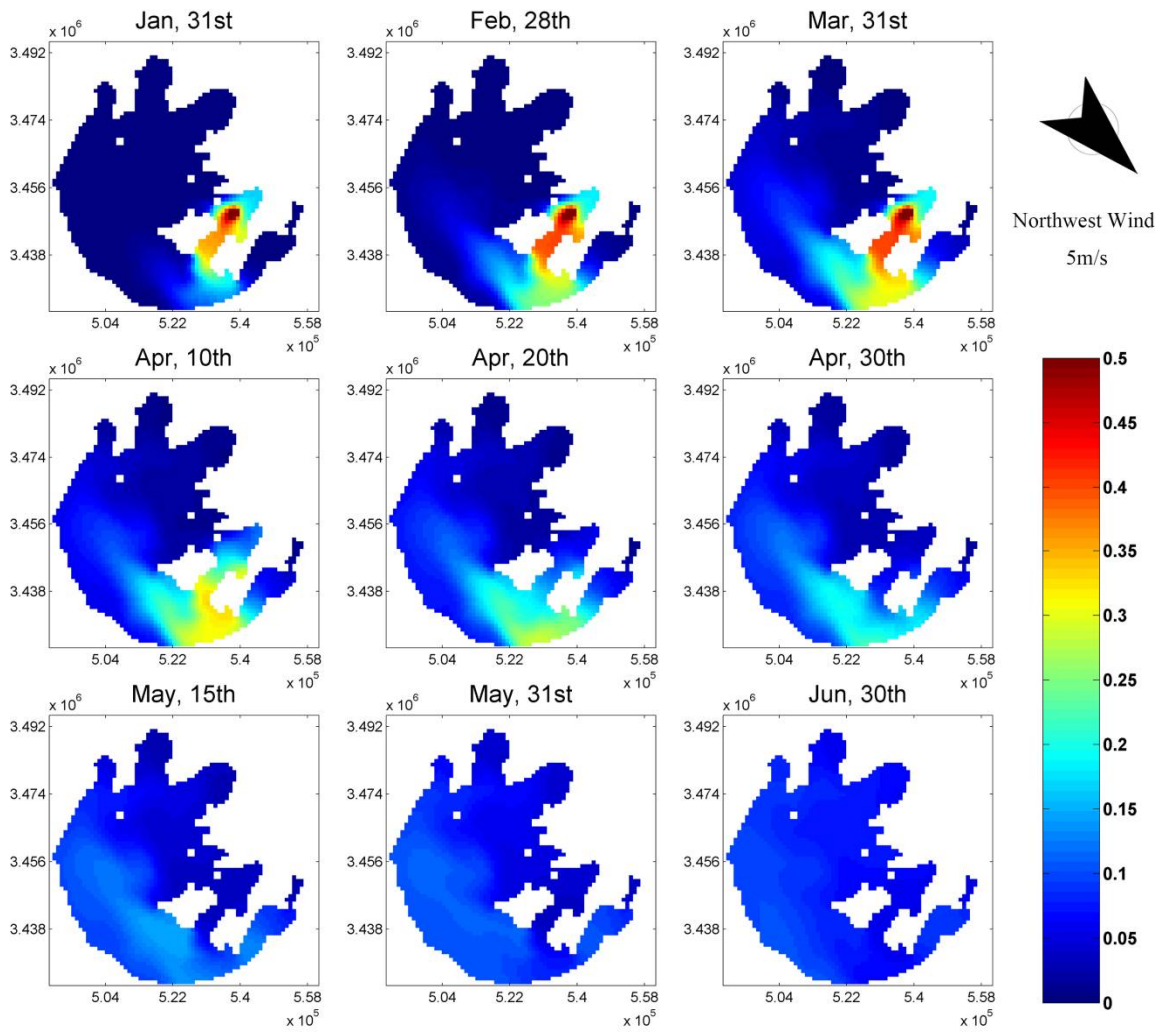


**Figure 16.** Time series of tracer concentration images, with the model driven by constant 5 m/s northwest wind. Unit in the figure is  $\text{kg}/\text{m}^3$ .

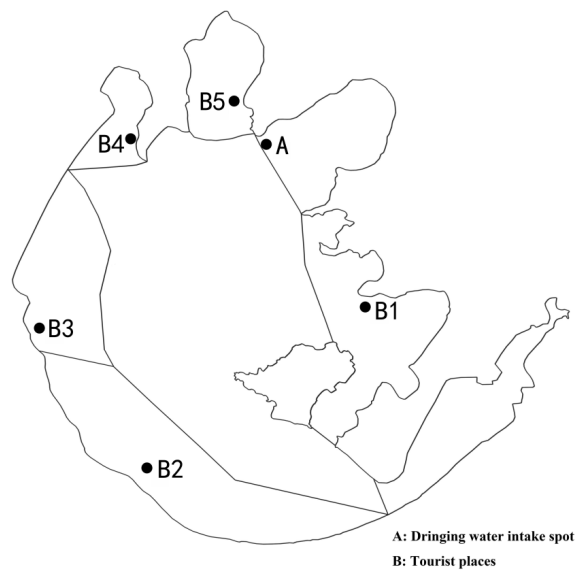


**Figure 17.** Important spots for pollution (tracer) release experiment analysis.

With constant northwest wind scenarios, which are represented as blue lines in Figure 18, the situation is similar. Tracers from Meiliang Bay reach location A first, however, the distance travelled in this situation is longer than tracer released in Gonghu Bay with southeast wind. Due to mixing and diffusion processes, the peak concentration at location A with northwest wind is smaller than that with southeast wind. Water from Zhushan Bay and Center Zone arrives later, and introduces delayed concentration peaks. Specially to be noted, tracers released from Dongtaihu Bay show less influence due to longer travel distance, and weak hydrodynamics inside Dongtaihu Bay.

For lake authorities, the analysis of hydrodynamic circulation with tracer experiments under constant wind conditions may provide a quick tool to assess emergency pollution impact on critical area before carrying out a more complicated hydrodynamic and water quality model. Also, the model could help to design temporary observation locations based on the environmental conditions. For example, given the emission location at Eastepigeal Zone and southeast wind, an observation points located to the north of Xishan Island is more useful than to the south.

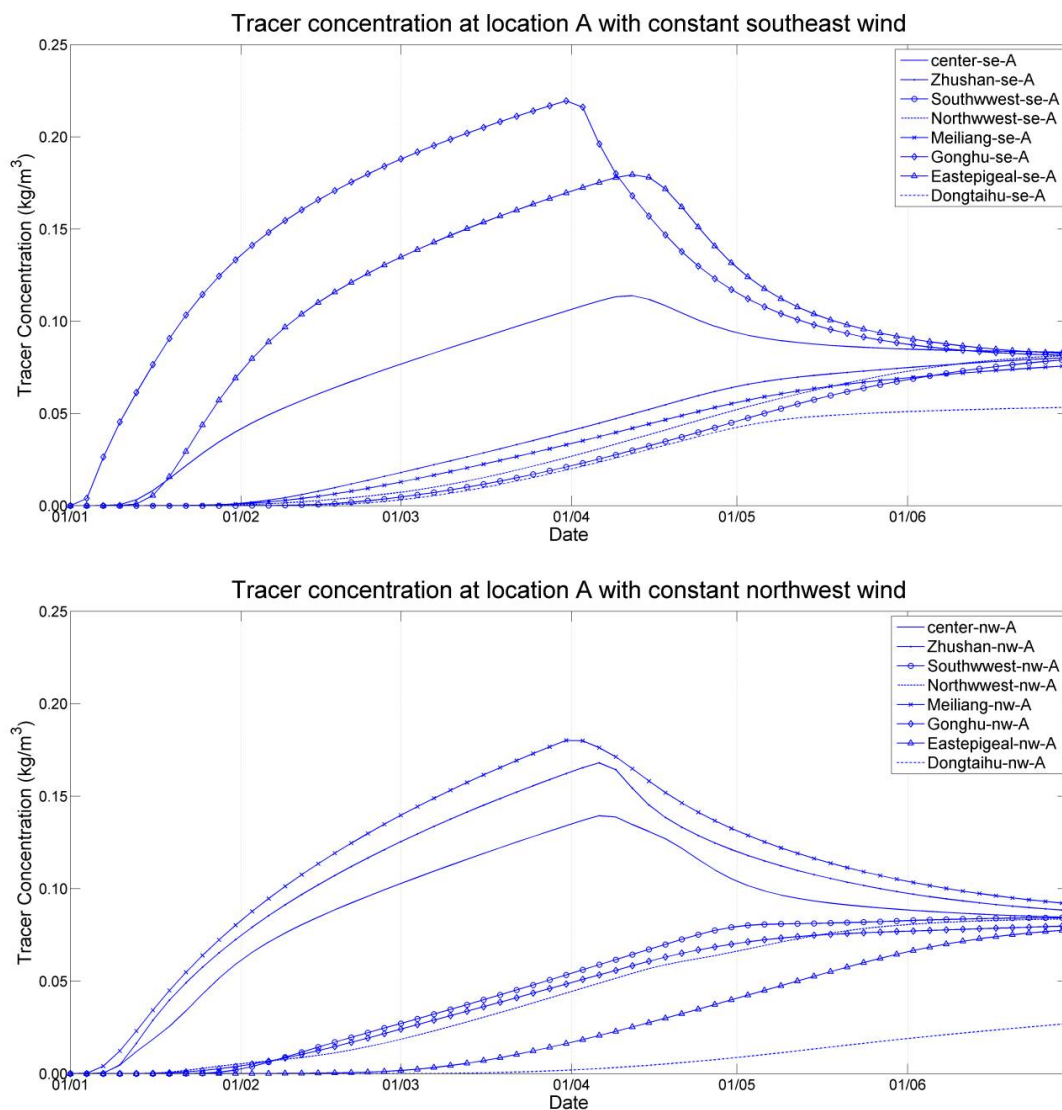


**Figure 18.** Tracer concentration at location A with different tracer release spot, the upper subplot shows tracer concentration with constant 5 m/s southeast wind condition, while the lower subplot describes the northwest wind condition. To make the plot clearer, data are extracted per 3 days from the model results.

### 5.5. Is Large-Scale Water Transfer Effective?

Diluting and flushing of Taihu Lake with water pumped from the Yangtze River has been the largest engineering intervention to improve water quality in Taihu Lake after 2007. Previous studies with field data collection have been carried out to identify the variation in water quality and biological indices before and after the water transfer. Results show that the effectiveness of water transfer project remains of concern. Positive effects occurred only in parts of Taihu Lake, while in some other areas, water quality even worsened [29,30,43].

To investigate the hydrodynamic circulation condition change due to the project, numerical experiments are carried out using the original discharge data of 2008, and the water transfer rate from literature (Table 1 in [30]). The water transfer in 2008 lasted from 23 January to 9 June, with a total transferred water volume of 870.2 million  $\text{m}^3$ , which is around 6.7 million  $\text{m}^3/\text{d}$ .

Model results suggest that, except for Dongtaihu Bay and Gonghu Bay, no significant change in hydrodynamic circulation condition occurred with and without water transfer. Total discharges of Gonghu Bay and Dongtaihu Bay are shown in Figure 19.

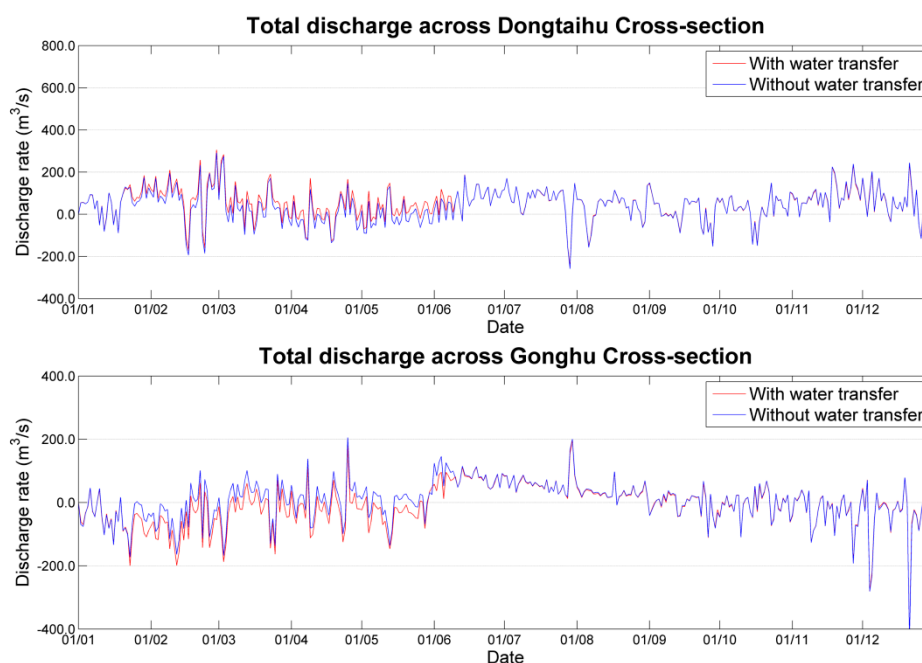


**Figure 19.** Total discharge of Gonghu Bay and Dongtaihu Bay. The red lines refer to the reference case, while blue line represents scenarios without water transfer.

For other open cross-sections, such as southwest and northwest, volume exchanges slightly fluctuate, but for the entrance cross-sections of semi-closed subbasins like Meiliang Bay, the total discharge remains the same.

Model results of total volume exchanges across the cross-sections show that transferred water neither significantly changed the water amount within each subbasin nor enhanced the volume exchange between subbasins. However, it indeed stimulated the hydrodynamic circulation in Gonghu Bay and Dongtaihu Bay.

Although the water transfer project contributes little to changing the total volume in most subbasins, hydrodynamic circulations still transfer and mix water persistently throughout the lake. Considering that the water transferred from the Yangtze River contains less nutrient or pollution than the average of Taihu Lake, with the amount of transferred water that stayed in the subbasins, the nutrient concentration would consequently change; a tracer experiment is conducted to further elucidate the redistribution of transferred water. This scenario lasts for the entire year of 2008, and

tracers are continuously released on Wangyu River boundary at a concentration of  $5 \text{ kg/m}^3$  between 23 January and 9 June 2008.

Model results are shown in Figure 20. As can be observed from the top right subplot, after 129 days on 9 June, a large amount of transferred water has already reached Gonghu Bay, Meiliang Bay, and Center Zone. Later, the tracers move southeastwards before they leave the lake from Taipu River. To be especially noticed, almost no tracers pass through the entrance of Zhushan Bay, making tracer concentration virtually zero inside this subbasin. Volume exchange between Zhushan Bay and other parts of Taihu Lake is more severely blocked, partially due to a weak hydrodynamic circulation near the entrance of the subbasin.

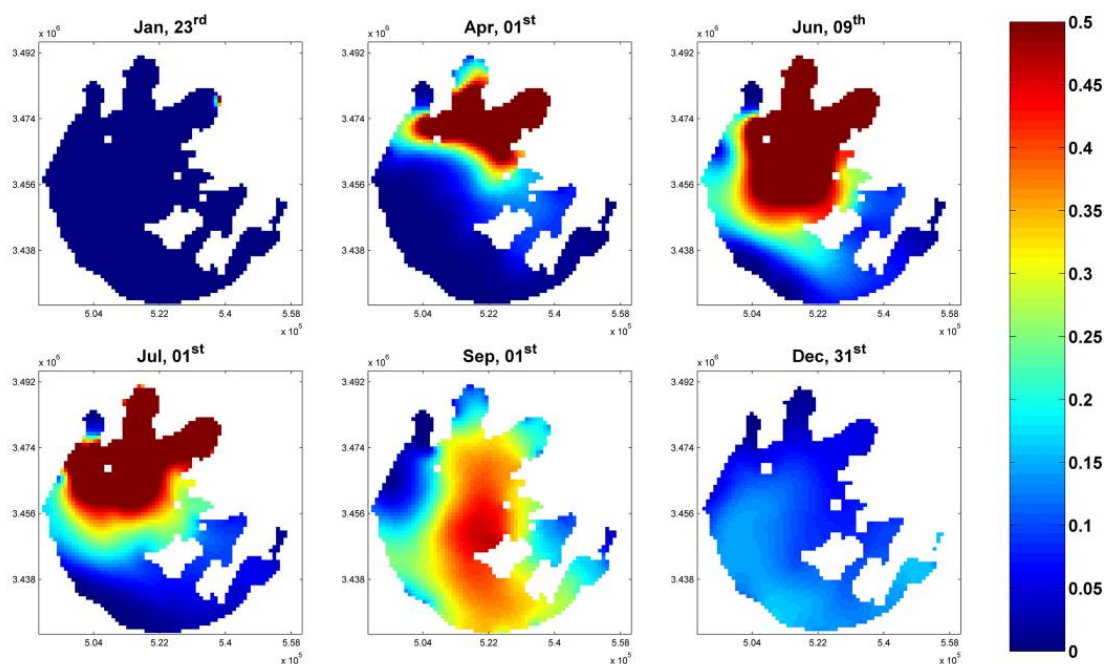


**Figure 20.** Time series of depth-averaged tracer concentration images, unit in map is  $\text{kg/m}^3$ . To conclude, the water transfer project in Taihu Lake did not significantly stimulate the hydrodynamic circulation or volume exchange between subbasins. However, tracer scenarios illustrate the project did succeed in redistributing the clearer transferred water throughout the lake, especially in some semi-closed subbasins, like Meiliang Bay and Dongtaihu Bay.

## 6. Conclusions

Wind-induced hydrodynamic circulations and associated transport and mixing processes in large shallow lakes play a significant role in their environmental and ecological processes. Knowledge of these physical mechanisms helps understanding, with the hope to solve eutrophication problems like algae blooms, which happen increasingly frequently in large shallow lakes, like Taihu Lake. Previous studies emphasized mostly the environmental, biological, and ecological aspects of eutrophication problems. However, the driving forces of nutrient transport, algae scums, pollutant mixing, and the underlying physical processes, such as wind-driven or anthropological horizontal circulation, are usually overlooked, but they might be key factors leading to algae blooms, and hitherto ambiguous. In this study, hydrodynamic circulation in shallow lakes is defined as the large-scale movement of water in the lake basin. A three-dimensional, numerical Delft3D model of Taihu Lake, driven by steady and/or unsteady wind, river discharge, rainfall, and evaporation, is used to quantitatively illustrate the complex hydrodynamic circulation and their effects in transporting and mixing within the lake.

A relative stable circulation pattern is found to be formed after 2 days, on average, with steady wind, where the overall hydrodynamic circulation structure, i.e., direction, intensity, and position, is

determined by wind direction, wind speed, and initial water level. Vertical variations of horizontal velocity are found to be related to the relative shallowness of water depth. In the shallow marginal area, flow at the bottom and surface layers has the same direction, and the surface flow has a larger velocity, while in the deeper area, the bottom flow reverses, opposite to the wind direction and with a larger velocity. Volume exchange between subbasins, influenced by wind speed and initial water level, differs due to the complex topography and irregular shape. With unsteady wind, these findings are still valid to a high degree. Vertical variations in hydrodynamic circulation are found to be very important in explaining the surface accumulation of algae scums in Meiliang Bay in summer. Vorticity of current velocity, as the key indicator of hydrodynamic circulation, is determined by wind direction, bathymetry gradient, and water depths, while the maximum change of velocity vorticity happens when wind direction and bathymetry gradient are perpendicular to each other. Furthermore, we use Lagrangian-based tracer tests to estimate emergency pollution/leakage effects and to evaluate water transfer effects. One emergency pollution leakage point is added to the model to demonstrate the effect on five tourism hotspots and one drinking water intake point, suggesting that the model application may serve as an operational management tool. The water transfer project shows that even a large-scale water transfer (about 1/5 volume of total lake volume in 138 days from Yangtze) does not alter the hydrodynamic circulation and volume exchanges between subbasins significantly, but it succeeds to transport and mix the imported Yangtze River water to the majority of Taihu Lake area.

This study may well be extended further to provide insight into the spatial and temporal biological process corresponding to wind induced hydrodynamic circulation in Taihu Lake, and similar large shallow lakes, to support ecologically sound design and implementation for lake restoration.

**Author Contributions:** S.L., Q.Y. and M.J.F.S. conceived this research theme; S.L. and Q.Y. developed the methodology, set up and calibrated the numerical model and did the result analysis; S.W. provided the essential data; S.L. and Q.Y. wrote the original draft; M.J.F.S. and S.W. revised the manuscript.

**Funding:** This research was funded by Chinese International S&T Cooperation Program of China grant number (ISTCP project No. 2015DFA0100) and China Scholarship Council (CSC) (201407720008).

**Acknowledgments:** The authors would like to thank TBA for the tributary discharge data and monitoring station water level data.

**Conflicts of Interest:** The authors declare no conflict of interest.

## Appendix Cross-Section Discharge Calculation

Eight cross-sections are placed at the entrance of the subbasins (Figure 1) to compute volume exchange between subbasins. In this study, volume exchange between subbasins is calculated as the total amount of water that transports across the cross-sections by adding up the perpendicular horizontal discharge rate components of all the grid cells at the entrance cross-sections of each subbasin. For each grid cell, the discharge model result is set at the cell center.

In Delft3D, the horizontal spatial distribution of the simulation grid uses two perpendicular  $m$  and  $n$  axis. An example of volume exchange calculation is shown in Figure A1. The cross-section is along the  $n$  direction at  $n_0$ .

Total volume exchange is calculated as:

$$\text{Volume exchange} = \sum_{k=1}^5 \sum_{m=m_i}^{m_{i4}} Q_{m,n_0k} \times S_{m,n_0k}, \quad (\text{A1})$$

where  $k$  is the vertical layer index with 1 at the surface layer and 5 at the bottom.  $m_i$  and  $m_{i4}$  are the begin and end grid index,  $Q_{m,n_0k}$  is the corresponding perpendicular component of horizontal discharge and  $S_{m,n_0k}$  is the grid size which could be calculated with the grid size  $l$ , with water depth  $d$  and water level  $\zeta$ .

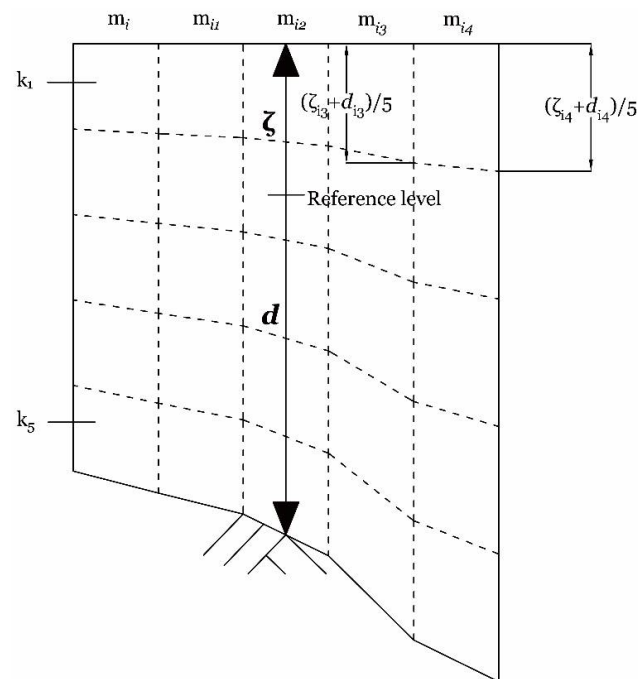


**Figure A1.** Vertical cross-section layout for volume exchange calculation.

## References

- Smith, V.H.; Tilman, G.D.; Nekola, J.C. Eutrophication: impacts of excess nutrient inputs on freshwater, marine, and terrestrial ecosystems. *Environ. Pollut.* **1999**, *100*, 179–196. [[CrossRef](#)]
- Paerl, H.W.; Xu, H.; McCarthy, M.J.; Zhu, G.; Qin, B.; Li, Y.; Gardner, W.S. Controlling harmful cyanobacterial blooms in a hyper-eutrophic lake (Lake Taihu, China): The need for a dual nutrient (N and P) management strategy. *Water Res.* **2011**, *45*, 1973–1983. [[CrossRef](#)] [[PubMed](#)]
- Janssen, A.B.G.; Teurlincx, S.; An, S.; Janse, J.H.; Paerl, H.W.; Mooij, W.M. Alternative stable states in large shallow lakes? *J. Great Lakes Res.* **2014**, *40*, 813–826. [[CrossRef](#)]
- Codd, G.A.; Lindsay, J.; Young, F.M.; Morrison, L.F.; Metcalf, J.S. Harmful Cyanobacteria. In *Harmful Cyanobacteria*; Huisman, J., Matthijs, H.C.P., Visser, P.M., Eds.; Springer: Berlin, Germany, 2005; pp. 1–23.
- Chen, Q.; Zhang, C.; Recknagel, F.; Guo, J.; Blanckaert, K. Adaptation and multiple parameter optimization of the simulation model SALMO as prerequisite for scenario analysis on a shallow eutrophic Lake. *Ecol. Model.* **2014**, *273*, 109–116. [[CrossRef](#)]
- Le, C.; Zha, Y.; Li, Y.; Sun, D.; Lu, H.; Yin, B. Eutrophication of lake waters in China: Cost, causes, and control. *Environ. Manag.* **2010**, *45*, 662–668. [[CrossRef](#)] [[PubMed](#)]
- Gulati, R.D.; Pires, L.M.D.; Van Donk, E. Lake restoration studies: Failures, bottlenecks and prospects of new ecotechnological measures. *Limnologia* **2008**, *38*, 233–248. [[CrossRef](#)]
- Leira, M.; Cantonati, M. Effects of water-level fluctuations on lakes: An annotated bibliography. *Hydrobiologia* **2008**, *613*, 171–184. [[CrossRef](#)]
- Nutz, A.; Schuster, M.; Ghienne, J.-F.; Roquin, C.; Bouchette, F. Wind-driven waterbodies: a new category of lake within an alternative sedimentologically-based lake classification. *J. Paleolimnol.* **2018**, *59*, 189–199. [[CrossRef](#)]
- Jeppesen, E.; Søndergaard, M.; Meerhoff, M.; Lauridsen, T.L.; Jensen, J.P. Shallow lake restoration by nutrient loading reduction—Some recent findings and challenges ahead. *Hydrobiologia* **2007**, *584*, 239–252. [[CrossRef](#)]
- Paerl, H.W.; Hall, N.S.; Calandrino, E.S. Controlling harmful cyanobacterial blooms in a world experiencing anthropogenic and climatic-induced change. *Sci. Total Environ.* **2011**, *409*, 1739–1745. [[CrossRef](#)] [[PubMed](#)]
- Pastorok, R.A.; Ginn, T.C.; Lorenzen, M.W. *Evaluation of Aeration/Circulation as a Lake Restoration Technique*; Environmental Research Laboratory, Office of Research and Development, US Environmental Protection Agency: Washington, WA, USA, 1981.

13. Zarzuelo, C.; Díez-Minguito, M.; Ortega-Sánchez, M.; López-Ruiz, A.; Losada, M.T. Hydrodynamics response to planned human interventions in a highly altered embayment: The example of the Bay of Cádiz (Spain). *Estuar. Coast. Shelf Sci.* **2015**, *167*, 75–85. [[CrossRef](#)]
14. Dake, J.M.K.; Harleman, D.R.F. Thermal stratification in lakes: Analytical and laboratory studies. *Water Resour. Res.* **1969**, *5*, 484–495. [[CrossRef](#)]
15. Cooke, G.D.; Welch, E.B.; Peterson, S.; Nichols, S.A. *Restoration and Management of Lakes and Reservoirs*; CRC Press: Boca Raton, FL, USA, 2016.
16. Qian, J.; Zheng, S.; Wang, P.; Wang, C. Experimental study on sediment resuspension in taihu lake under different hydrodynamic disturbances. *J. Hydrodyn. Ser. B* **2011**, *23*, 826–833. [[CrossRef](#)]
17. Fragoso, C.R.; Motta Marques, D.M.L.; Ferreira, T.F.; Janse, J.H.; van Nes, E.H. Potential effects of climate change and eutrophication on a large subtropical shallow lake. *Environ. Model. Softw.* **2011**, *26*, 1337–1348. [[CrossRef](#)]
18. You, B.S.; Zhong, J.C.; Fan, C.X.; Wang, T.C.; Zhang, L.; Ding, S.M. Effects of hydrodynamics processes on phosphorus fluxes from sediment in large, shallow Taihu Lake. *J. Environ. Sci.* **2007**, *19*, 1055–1060. [[CrossRef](#)]
19. Józsa, J. On the internal boundary layer related wind stress curl and its role in generating shallow lake circulations. *J. Hydrol. Hydromech.* **2014**, *62*, 16–23. [[CrossRef](#)]
20. Wüest, A.; Lorke, A. Small Scale Hydrodynamics in Lakes. *Annu. Rev. Fluid Mech.* **2003**, *35*, 373–412. [[CrossRef](#)]
21. Boegman, L.; Loewen, M.R.; Hamblin, P.F.; Culver, D.A. Application of a two-dimensional hydrodynamic reservoir model to Lake Erie. *Can. J. Fish. Aquat. Sci.* **2001**, *58*, 858–869. [[CrossRef](#)]
22. Zhang, H.; Culver, D.A.; Boegman, L. A two-dimensional ecological model of Lake Erie: Application to estimate dreissenid impacts on large lake plankton populations. *Ecol. Model.* **2008**, *214*, 219–241. [[CrossRef](#)]
23. Hulot, F.D.; Rossi, M.; Verdier, B.; Urban, J.P.; Blottière, L.; Madricardo, F.; Decencièrre, B. Mesocosms with wavemakers: A new device to study the effects of water mixing on lake ecology. *Limnol. Oceanogr. Methods* **2017**, *15*, 154–165. [[CrossRef](#)]
24. Fenocchi, A.; Petaccia, G.; Sibilla, S. Modelling flows in shallow (fluvial) lakes with prevailing circulations in the horizontal plane: limits of 2D compared to 3D models. *J. Hydroinform.* **2016**, *20*. [[CrossRef](#)]
25. Hu, W.; Jørgensen, S.E.; Zhang, F. A vertical-compressed three-dimensional ecological model in Lake Taihu, China. *Ecol. Model.* **2006**, *190*, 367–398. [[CrossRef](#)]
26. Yu, Y.; Wang, X.; Yang, D.; Lei, B.; Zhang, X.; Zhang, X. Evaluation of human health risks posed by carcinogenic and non-carcinogenic multiple contaminants associated with consumption of fish from Taihu Lake, China. *Food Chem. Toxicol.* **2014**, *69*, 86–93. [[CrossRef](#)] [[PubMed](#)]
27. Chengxin, F.; Lu, Z.; Jianjun, W.; Chaohai, Z.; Guang, G.; Sumin, W. Processes and mechanism of effects of sludge dredging on internal source release in lakes. *Chin. Sci. Bull.* **2004**, *49*, 1853–1859.
28. Qin, B.; Zhu, G.; Gao, G.; Zhang, Y.; Li, W.; Paerl, H.W.; Carmichael, W.W. A drinking water crisis in Lake Taihu, China: Linkage to climatic variability and lake management. *Environ. Manag.* **2010**, *45*, 105–112. [[CrossRef](#)] [[PubMed](#)]
29. Hu, W.; Zhai, S.; Zhu, Z.; Han, H. Impacts of the Yangtze River water transfer on the restoration of Lake Taihu. *Ecol. Eng.* **2008**, *34*, 30–49. [[CrossRef](#)]
30. Li, Y.; Acharya, K.; Yu, Z. Modeling impacts of Yangtze River water transfer on water ages in Lake Taihu, China. *Ecol. Eng.* **2011**, *37*, 325–334. [[CrossRef](#)]
31. Zhang, H.; Hu, W.; Gu, K.; Li, Q.; Zheng, D.; Zhai, S. An improved ecological model and software for short-term algal bloom forecasting. *Environ. Model. Softw.* **2013**, *48*, 152–162. [[CrossRef](#)]
32. Hu, W. A review of the models for Lake Taihu and their application in lake environmental management. *Ecol. Model.* **2016**, *319*, 9–20. [[CrossRef](#)]
33. Li, Y.; Tang, C.; Wang, C.; Tian, W.; Pan, B.; Hua, L.; Lau, J.; Yu, Z.; Acharya, K. Assessing and modeling impacts of different inter-basin water transfer routes on Lake Taihu and the Yangtze River, China. *Ecol. Eng.* **2013**, *60*, 399–413. [[CrossRef](#)]
34. Smith, S.D.; Banke, E.G. Variation of the sea surface drag coefficient with wind speed. *Q. J. R. Meteorol. Soc.* **1975**, *101*, 665–673. [[CrossRef](#)]
35. Falconer, R.A.; George, D.G.; Hall, P. Three Dimensional Numerical Modelling of Wind-driven Circulation in a Shallow Homogeneous Lake. *J. Hydrol.* **1991**, *124*, 59–79. [[CrossRef](#)]

36. Nash, J.E.; Sutcliffe, J. V River Flow Forecasting Through Conceptual Models Part I—a Discussion of Principles. *J. Hydrol.* **1970**, *10*, 282–290. [[CrossRef](#)]
37. Willmott, C.J. On the validation of models. *Phys. Geogr.* **1981**, *2*, 184–194.
38. Rueda, F.J.; Schladow, S.G.; Monismith, S.G.; Stacey, M.T. On the effects of topography on wind and the generation of currents in a large multi-basin lake. *Hydrobiologia* **2005**, *532*, 139–151. [[CrossRef](#)]
39. Simionato, C.G.; Dragani, W.; Meccia, V.; Nuñez, M. A numerical study of the barotropic circulation of the Río de la Plata estuary: Sensitivity to bathymetry, the Earth’s rotation and low frequency wind variability. *Estuar. Coast. Shelf Sci.* **2004**, *61*, 261–273. [[CrossRef](#)]
40. Strub, P.T.; Powell, T.M. Wind-driven surface transport in stratified closed basins: Direct versus residual circulations. *J. Geophys. Res.* **1986**, *91*. [[CrossRef](#)]
41. Schoen, J.H.; Stretch, D.D.; Tirok, K. Wind-driven circulation patterns in a shallow estuarine lake: St Lucia, South Africa. *Estuar. Coast. Shelf Sci.* **2014**, *146*, 49–59. [[CrossRef](#)]
42. Laval, B.; Imberger, J.; Hodges, B.R.; Stocker, R. Modeling circulation in lakes: Spatial and temporal variations. *Limnol. Ocean.* **2003**, *48*, 983–994. [[CrossRef](#)]
43. Zhai, S.; Hu, W.; Zhu, Z. Ecological impacts of water transfers on Lake Taihu from the Yangtze River, China. *Ecol. Eng.* **2010**, *36*, 406–420. [[CrossRef](#)]



© 2018 by the authors. Licensee MDPI, Basel, Switzerland. This article is an open access article distributed under the terms and conditions of the Creative Commons Attribution (CC BY) license (<http://creativecommons.org/licenses/by/4.0/>).